RESEARCH ARTICLE

Intraseasonal Oscillations and Hydroclimate of Northern South America, Central America and Mexico

Alejandro Builes-Jaramillo[1] | Johanna Yepes[1] | Hernán D. Salas[2] | Juan M. Bedoya-Soto[3] | Paris Rivera[4] | Juliana Valencia[1] | Alejandra M. Carmona[5]

[1]Facultad de Arquitectura e Ingeniería, Institución Universitaria Colegio Mayor de Antioquia, Medellín, Antioquia, Colombia | [2]Facultad de Ciencias Exactas y Aplicadas, Instituto Tecnológico Metropolitano, Medellín, Colombia | [3]Corporación Universitaria Remington, Medellín, Colombia | [4]Universidad Mariano Gálvez, Ciudad de Guatemala, Guatemala | [5]School of Applied Sciences and Engineering, Universidad EAFIT, Medellín, Colombia

Correspondence: Alejandro Builes-Jaramillo (luis.builes@colmayor.edu.co)

Received: 21 August 2024 | **Revised:** 19 December 2024 | **Accepted:** 20 February 2025

Funding: This work was supported by Institución Universitaria Colegio Mayor de Antioquia, Project: FAI149.

Keywords: Kelvin waves | Madden–Julian oscillation | mixed Rossby-gravity waves | tropical easterly waves | tropical hydroclimatology

ABSTRACT

We examine the influence of intraseasonal variability (10–90 days) on hydroclimatic variables across Northern South America, Central America and Mexico. This variability is driven by planetary and tropical oscillations, including Kelvin waves, Tropical Easterly Waves, Mixed Rossby-Gravity Waves and the Madden–Julian oscillation, all of which display distinct signals in the wavenumber–frequency power spectra. Our findings reveal that intraseasonal variability accounts for 10%–35% of the total variance, depending on the specific location, with Kelvin waves being the largest contributors to the outgoing longwave radiation variance in the study region. Additionally, we observed positive and negative precipitation anomalies across the region associated with each oscillatory process, which can be linked to anomalies in moisture transport and convection within the atmospheric column. The Madden–Julian oscillation contributes 10%–12% of precipitation over continental areas, while Tropical Easterly Waves and Mixed Rossby-Gravity waves account for approximately 40% of the precipitation over the continent. These findings offer new insights into the spatial and temporal patterns within the region. A deeper understanding, diagnosis and prediction of this timescale are crucial for economic sectors such as agriculture, energy generation, risk management and water resources.

1 | Introduction

The intraseasonal variability lies between the time scale associated with weather forecasts (ranging from a few days up to around a week) and scales associated with climate predictions (seasonal, annual and longer time scales) (Lau and Waliser 2012). In particular, tropical intraseasonal variability refers to a wide spectrum of phenomena that includes quasi-periodic and non-periodic modes over synoptic (~1000 km, ~1–10 days) and global scales (~10,000 km, ~10–100 days) (Serra et al. 2014). The tropical intraseasonal variability includes the Tropical Easterly Waves (TEW) (2.5–12 days) (Valencia et al. 2024), Kelvin waves (KWs) (2.5–17.5 days) (Peyrillé et al. 2023), Equatorial Rossby Waves (10–48 days) (Wheeler and Kiladis 1999), Mixed Rossby-Gravity waves (MRG) (3–10 days) (Suhas et al. 2020) and the Madden–Julian oscillations (MJO) (30–90 days) (Zhang 2015),

Abbreviations: KW, Kelvin waves; MJO, Madden–Julian oscillation; MRG, mixed Rossby-gravity waves; TEWs, tropical easterly waves.
Alejandro Builes-Jaramillo, Johanna Yepe, and Hernán D. Salas contributed equally.

which impact regional weather, short-term climate patterns, and atmospheric chemical transports, among others (Serra et al. 2014; Dominguez et al. 2020; Peyrillé et al. 2023; Teruya et al. 2024).

The TEWs are the main synoptic system observed in tropical regions and their importance lies in two fundamental reasons: (i) the transport of humidity and its relationship with convective rain (Fink and Reiner 2003; Gu et al. 2004); and (ii) their influence on tropical processes at different scales (Pasch and Avila 1994; Berry and Thorncroft 2005; Cornforth et al. 2017). Seasonally, TEWs show stronger activity during June to November (Serra et al. 2010). TEWs influence precipitation and streamflow in Northern South America (NSA) (Dominguez et al. 2020; Cárdenas et al. 2017; Salas et al. 2022). They have been shown to significantly impact both diurnal and seasonal rainfall, modulated by large-scale climatic oscillations such as El Niño Southern Oscillation (ENSO). On seasonal scales, Dominguez et al. (2020) find that TEWs can account for up to 50% of seasonal rainfall, particularly in northern South America, and highlight the role of ENSO in modulating the frequency of TEWs with an increase (decrease) of TEWs activity during La Niña (El Niño) conditions. Moreover, at diurnal scales, TEWs significantly enhance the frequency of rainfall over Costa Rica during convectively active periods while the intensity of rainfall varies more subtly with the TEWs phases, where active conditions tend to slightly delay the diurnal peak intensity and extend the duration of heavier rainfall (Wiggins et al. 2023).

KWs are one of the most dominant atmospheric waves in the tropics (Matsuno 1966) and characterised by periods of 15 days, length scales between 20,000 km and 40,000 km (numbers of zonal waves 2 and 1) and vertical scales ranging from 6 to 10 km (Lau and Waliser 2012; Herman et al. 2016; Chien and Kim 2023). KW influence global atmospheric circulation, zonal wind, temperature and residual meridional circulation (Koval et al. 2023). They contribute to the formation of dynamic and temperature regimes in the middle and upper atmosphere (Koval et al. 2023). Furthermore, KWs show stronger activity during westerly quasi-biennial oscillation (QBO) phases (Fathullah et al. 2017) and ENSO during its warm phase (KW with Pacific origin) (Mayta et al. 2021). Besides, KW have a stronger seasonal cycle with pronounced patterns during JJA and SON (Tiyas et al. 2022). Specifically, Convectively Coupled Kelvin Waves (CCKW) are associated with convection and extreme precipitation (Senior et al. 2023; Ferrett et al. 2020; Straub and Kiladis 2002). Moreover, CCKW modulate the diurnal cycle of precipitation (Lubis and Respati 2021) and synoptic time scale streamflow variability (Salas et al. 2022). Also, CCKW superimposed with MJO and Rossby waves lead to devastating floods (Latos et al. 2021). Over South America, CCKW shift their amplitude and vertical structure due to MJO altering precipitation patterns (Guo et al. 2014). Over the Amazon region, KW originating from the Pacific Ocean, arising from South American extratropics, and triggered by pre-existing convection contribute to 40%, 35% and 25% of precipitation events, respectively (Mayta et al. 2021).

Likewise, Equatorial Rossby Waves, Equatorial Inertia-Gravity Waves and MRG are important in tropical dynamics due to their coupling and effect on different climatic variables (Nakamura and Takayabu 2022a, 2022b; Fahrin et al. 2024; Gelbrecht et al. 2018; Suhas et al. 2020), the initiation of cyclonic activity (Latos et al. 2023; Feng et al. 2023) and the interaction between waves (Takasuka and Satoh 2020; Takasuka et al. 2021). Hereafter, we will focus on MRG waves, which exhibit westward propagation (Hendon and Liebmann 1991; Kiladis et al. 2016) and are characterised by symmetrical cross-equatorial meridional winds over the Pacific during boreal summer and fall (Suhas et al. 2020). Furthermore, MRG exhibit a mixing dynamics of Rossby and inertia-gravity waves, which contributes to the formation of tropical depressions and cyclones (Mahó et al. 2024; Aiyyer and Molinari 2003). They are influenced by dynamic and convective backgrounds, with increased frequency during La Niña and varying altitude based on vertical wind shear (Feng et al. 2016), and causing some disruptions over the QBO (Lin et al. 2022). While many studies focus on convectively coupled MRG waves (Wheeler and Kiladis 1999), some regions show weak convection-circulation coupling (Chen et al. 2016). Their seasonality is marked from May to October, with significant MRG events associated with extratropical disturbances (Shreya and Suhas 2024).

The MJO is described as an oceanic-atmospheric process that exhibits coherent eastward propagation along the equator with a quasi-periodicity between 40 and 50 oscillation days or 30–60 days (Lau and Waliser 2012; Li 2014; Zhang et al. 2020; Lin 2022). The MJO influences precipitation patterns and atmospheric circulation across South America and Central America (das Chagas Vasconcelos Junior et al. 2021; Peatman et al. 2014; Grimm 2019; Seiki et al. 2021). This oscillation impacts the South American monsoon during its active season (December–February), enhancing precipitation anomalies during the MJO Phases 3 and 4 (Alvarez et al. 2016). Furthermore, the MJO modulates rainfall in remote areas of the Southern Hemisphere by triggering tropical and extratropical wave trains, which lead to intensify precipitation anomalies over South America during the Phases 1 and 4 of the MJO and the easterly QBO (Sena et al. 2022). The MJO increases average daily precipitation by more than 30% in relation to climatology and doubles the frequency of extreme events over central-east South America and the South Atlantic Convergence Zone (SACZ) (Sena et al. 2022). Moreover, the MJO affects the Pacific Ocean Walker Circulation's descending branch, which is located near Western Tropical South America, driving zonal and vertical motions that influence regional precipitation (Recalde-Coronel et al. 2020). Additionally, the MJO produces a region of enhanced precipitation that travels eastwards along the Equator, perturbing both tropical and high-latitude winds. This modulation of winds contributes to extreme weather events, such as flooding and heat waves, across Central America (Maloney et al. 2019).

While existing global studies shed light on the influence of intra-seasonal processes on precipitation in diverse regions (Worku et al. 2020; Lawton et al. 2022; Gelbrecht et al. 2018; Recalde-Coronel et al. 2020), a significant gap exists in understanding the intricate interplay among KW, MRG, TEWs and the MJO in Central America, Northern South America and Mexico. This endeavour can significantly contribute to multidisciplinary knowledge, bridging the gap between

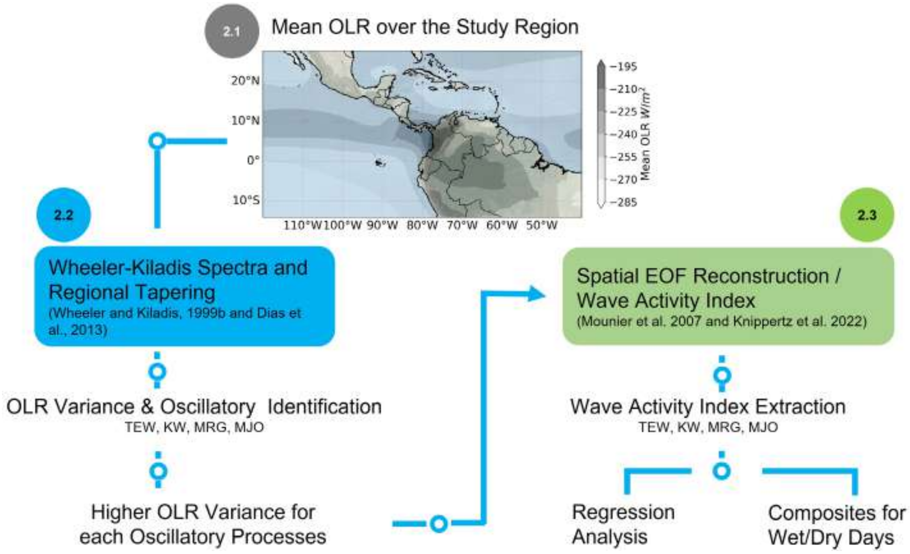

FIGURE 1 | Methodological scheme of the present work. Each section is labelled with a numbered circle, illustrating the sequence from filtering techniques used to extract OLR anomalies for each wave frequency, to the methods for identifying wave activity and compositing key times. [Colour figure can be viewed at wileyonlinelibrary.com]

atmospheric systems and local events (Tarasova et al. 2019). The purpose of this study is (i) to characterise the main intraseasonal oscillatory patterns over Northern South America, Central America and Mexico, (ii) to provide evidence of the influence of the main intraseasonal oscillations on precipitation in the region of study and (iii) to analyse the spatial structure of oscillations and their influence on the hydroclimate of the region of study.

2 | Datasets and Methodology

Our approach is based on the filtering of the main atmospheric oscillatory processes at the intraseasonal timescale in the tropics. To this end, we use the Wheeler–Kiladis Space-Time Spectra and Regional Tapering methods over the outgoing longwave radiation (OLR) in the study region for the 1981–2022 period. Once we computed the OLR anomalies in each one of the filtering bands, we performed a Spatial Empirical Orthogonal Function and OLR anomaly reconstructions based on the first two SEOFs. With this reconstruction, we extract standardised OLR anomalies as indices of oscillatory activity in the regions with greater OLR variance in each filtering band. Indices are then used to perform a composite analysis based on the dates of oscillatory activity (Figure 1).

2.1 | Study Region and Datasets

Our study region spans from 120° W–40° W; 30° N–15° S, encompassing Mexico, Central America and Northern South America (Figure 1, top panel). For this region, we use daily data from the ERA5 atmospheric reanalysis (Hersbach et al. 2019) for the following variables: OLR, zonal and meridional wind speeds at 850 hPa, specific humidity, vertically integrated moisture divergence (VIMD), vertical integrals of eastward and northward water vapour flux, and daily precipitation. To contrast the results obtained with the ERA5 precipitation dataset, we used daily precipitation from the Climate Hazards Group InfraRed Precipitation with Station—CHIRPS (Funk et al. 2015) which provides insights with a complementary dataset over the continental region, the analysis made with this dataset is included in Supporting Information.

2.2 | Wave Number–Frequency Power Spectra and Fourier Filters

To understand the main tropical atmospheric phenomena affecting precipitation variability in the study area, we analysed the regional frequency–wavenumber power spectra of ERA5 OLR using the method developed by Wheeler and Kiladis (1999). This approach, combined with the regional tapering approach from Dias et al. (2013), helped identify the tropical wave phenomena responsible for precipitation variability in the region. Specifically, we focused on the NSA, covering the longitudinal sector from 160° W to 20° E. To achieve a smooth synoptic signal distribution and reduce intraseasonal noise, we used 64-day window segments overlapping by 13 days and applied a Hann window, as in Huaman et al. (2020). We filtered the ERA5 OLR data to isolate the variability linked to the KW, MRG, TEWs and MJO waves coupled with convection. This was done using inverse Fourier transforms, keeping only the variability within the frequency–wavenumber boxes associated with each wave, following Wheeler and Kiladis (1999) and using boxes similar to Kiladis et al. (2009). The filtered data were then used to map the variance distribution and its annual cycle for each wave in the study region.

2.3 | Waves Structures and Their Association With Hydroclimatic Variables

We use composite analysis based on Mounier et al. (2007) and linear regression analysis according to Knippertz et al. (2022)

to elucidate the relationship between the intra-seasonal waves and the hydro-climatic fields. The composite analysis begins with a spatial EOF analysis for the period of analysis on the wave-filtered OLR values over the study region. We select only PC1 and PC2, after using the Scree test (Cattell 1966) and the North et al. (1982) rule of thumb as proposed by (Mounier et al. 2007), as they are the most important modes to represent the filtered intraseasonal variance. Furthermore, this selection enables us to focus on the main modes of intraseasonal waves, removing some background signal or noise retained in the filtering procedure (Mounier et al. 2007; Sakaeda et al. 2020) Particularly, these two first eigenvectors are in spatial quadrature and depict an approximate wavelength for the wave types. Furthermore, it is possible to build a new OLR anomalies field by using combined SEOF1 and SEOF2 reconstruction (hereafter "SEOF12").

Then, we can obtain an OLR index of each wave based on the SEOF12 OLR anomalies reconstruction over a region defined based on the OLR variance found in Section 3.1. This index corresponds to an average time series in the rectangular area that is extracted from the OLR anomaly field reconstructed for each wave (SEOF12). For this end, the regions based on the OLR variance are: (i) TEWs (40° W–50° W;5° N–10° N); (ii) KWs (100° W–120° W;2° N–10° N); (iii) MRGs (100° W–118° W;5° N–8° N) and (iv) MJOs (110° W–120° W;8° N–12° N).

Specifically, the process to synthesise the activity of each oscillation is structured in the following steps: (1) Decompose each filtered OLR field for MJO, TW, KW and MRG using SEOFs; (2) reduce the dimensionality of each filtered field retaining the variance of the first two SEOFs modes; (3) use the filtered and dimensionality reduced field to extract the time series that correspond to the cells contained in the key region identified for each wave; (4) average and standardise the time series that is finally the SEOF12 index of each wave.

Moreover, we designate a wet (dry) wave phase when the reconstructed SEOF12 OLR index is negative (positive), meaning a higher (weaker) convective activity in the base region. The wet (dry) cases have been selected when the standardised reconstructed OLR index is minimum (maximum) and weaker (higher) than minus (plus) 1.5. Then, with the dates provided by the SEOF12 OLR index, we carry out composites of the deseasonalised fields of interest (e.g., precipitation, VIMD, total wind speed (W), vertically integrated eastward and northward water vapour fluxes, which are computed based on the key times associated to the wet (dry) cases found for each wave type. Those results do not consider time lags and are presented as maps including the statistical significance using a *t*-test.

3 | Results

3.1 | Wave Number–Frequency Power Spectrum

Figure 2 presents the regional wave number–frequency power spectrum of the symmetric and antisymmetric components of ERA5 OLR for a region centred in Northern South America. This figure illustrates the ratio between the raw power and the power of a smoothed red noise background spectrum, with contours starting at 1.1 above the background level. The figure reveals a strong signal above the background in the spectral regions associated with KWs, MRG waves, easterly waves (EWs) and the MJO. The boxes in Figure 2 represent the wave number–frequency regions corresponding to these waves, which are used for filtering, as described by Kiladis et al. (2009). This figure provides a clear view of the dominant tropical wave phenomena in the study area. The presence of these waves indicates their significant role influencing the variability of OLR in the region. By identifying these spectral regions, we can better understand the contributions of each wave type to intraseasonal variability in the region. This approach enables the isolation and analysis of specific wave-related variabilities in the OLR data.

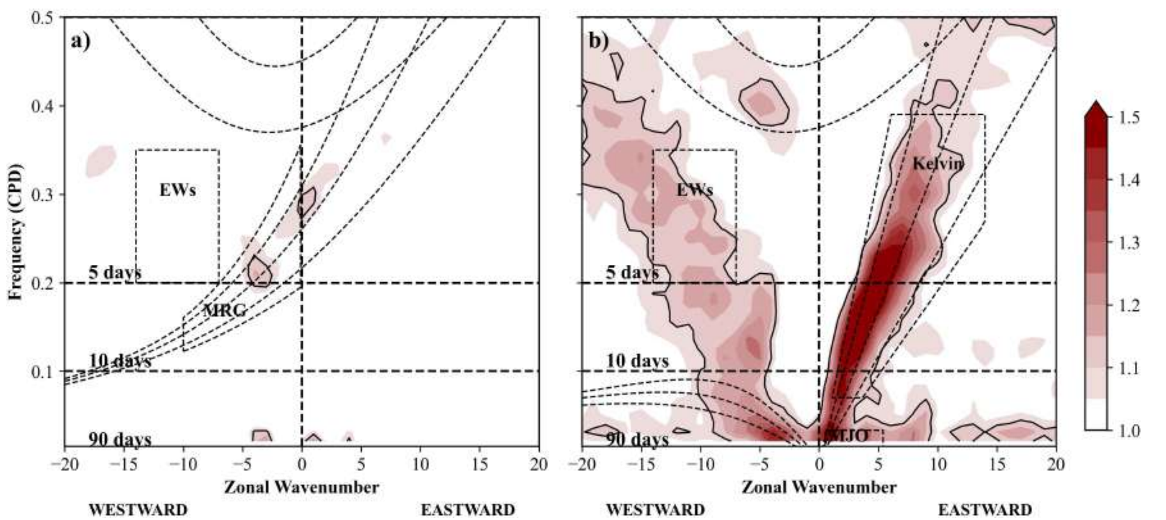

FIGURE 2 | Regional wave number–frequency power spectrum of the (a) symmetric and (b) antisymmetric component of ERA5 OLR, plotted as the ratio between raw power and the power in a smoothed red noise background spectrum. Light dotted lines show the dispersion curves for the Matsuno solutions to equatorial-trapped waves. Boxes represent regions of wave number–frequency filtering for the Kelvin waves, Mixed Rossby-Gravity (MRG) waves, Easterly waves (EWs), and Madden–Julian oscillations (MJOs). The dispersion curves (dashed lines) denote equatorial wave dispersion curves equivalent depths of $h = 8$, 12, 25, 50 and 90 m. [Colour figure can be viewed at wileyonlinelibrary.com]

3.2 | OLR Variance

Figure 3 shows the total variance of OLR for the period 1981–2022, which exhibits the highest values over northern South America (northernmost Colombia and the Colombian Pacific western coast), Central America, the eastern Pacific Ocean (around the latitude 10° N), and South-eastern South America (over the Amazon River basin). At intra-seasonal time scales, the variance explained by TEWs, KWs, MRGs, and MJOs constitutes around 16% of the total variance for all the study regions. From this 16% intraseasonal variance, each wave type's contribution is as follows: KWs are the biggest contributor with 37%, followed by the MJO with 23%, MRG with 20%, and TEWs with 15% of the total variance, respectively.

Conversely, lower variance in OLR was observed in the tropical Pacific and Atlantic Oceans, both oceanic regions, and at the continental level in northern and central Mexico and northern South America. The minimum variance observed in these locations could be related to various factors. In the case of the tropical Pacific and Atlantic, the presence of warm and stable waters likely contributes to lower variability in longwave radiation. These regions typically experience more uniform atmospheric conditions with fewer abrupt changes in OLR. Regarding continental areas like Mexico and northern South America, factors such as topography and land cover can influence OLR variability. Mountain ranges or dense vegetation may alter radiation distribution, reducing variability. Additionally, cloud cover, atmospheric humidity, and stability may also play roles, creating

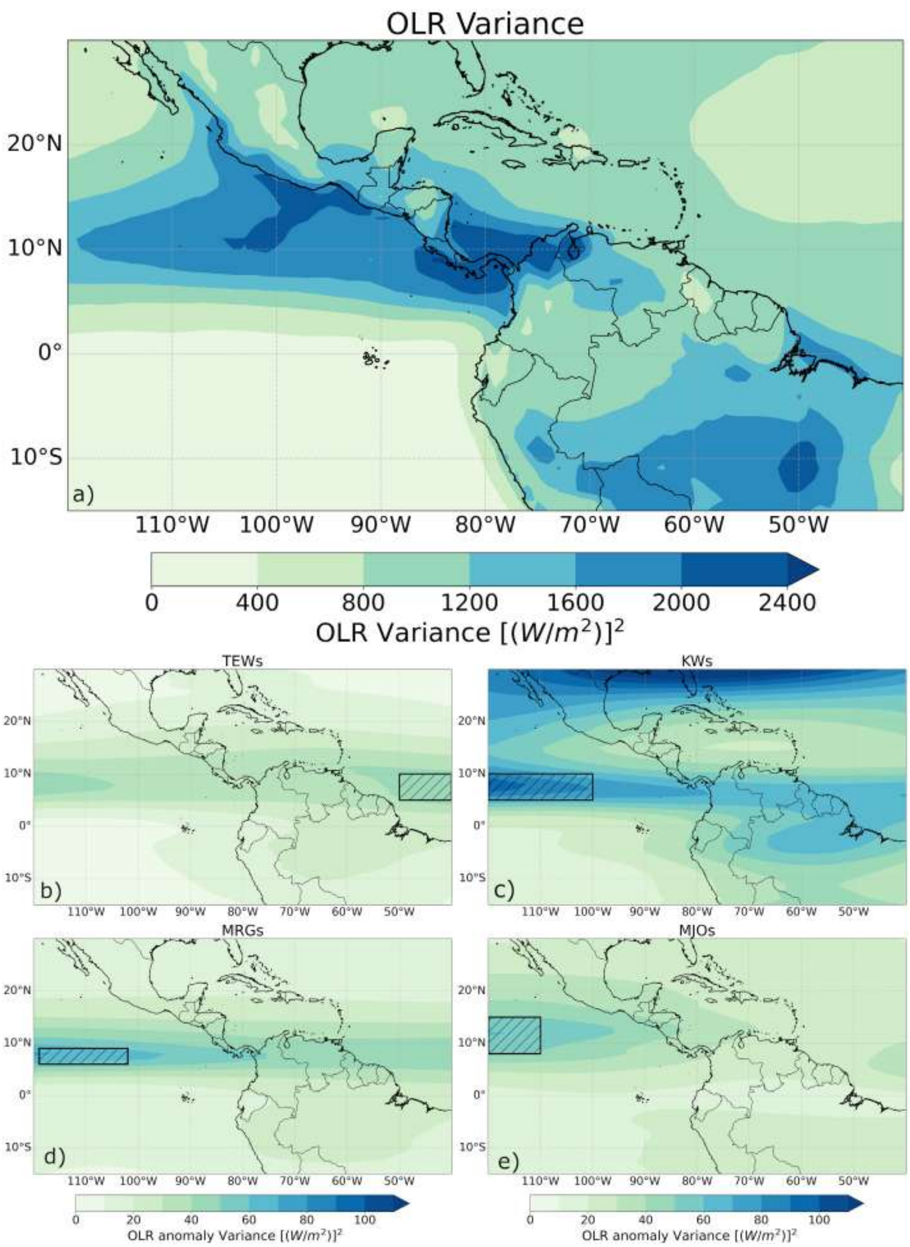

FIGURE 3 | (a) Variance of the unfiltered OLR over the region of study. The variance of the filtered OLR over the study region at frequency bands associated with intraseasonal oscillations: (b) Tropical Easterly Waves (TEWs), (c) Kelvin waves (KWs), (d) Mixed Rossby-Gravity (MRGs) and (e) Madden–Julian oscillations (MJOs). The base regions for the OLR reconstructions are depicted in dashed rectangles. [Colour figure can be viewed at wileyonlinelibrary.com]

more stable and predictable atmospheric conditions, thus reducing longwave radiation variability (Smith and Rutan 1994; Fung et al. 1984).

The Figure 3 also shows the desaggregated variance of the OLR anomalies for each intraseasonal oscillation associated with TEWs, KWs, MRGs, and MJOs, separately. The filtered OLR at time scales of the TEWs exhibits its higher variance in a region of the tropical Atlantic (40° W–50° W;5° N–10° N), the KWs over the tropical Pacific Ocean (100° W–120° W;2° N–10° N), the MRGs over the tropical Pacific (100° W–118° W;5° N–8° N), and the MJOs show their maximum variance in the Pacific Ocean (110° W–120° W;8° N–12° N). It is important to mention that all intraseasonal tropical waves exhibit high variance values over the Pacific Ocean around 10° N.

These results align with the analysis by Salas et al. (2022), who demonstrated that the highest variance is associated with KWs during June–July–August in northern South America. Additionally, our findings highlight two significant regions for KW over South America: the Eastern Pacific and the Amazon. These regions are consistent with previous studies (Liebmann et al. 2009; Mayta et al. 2021) identifying them as Kelvin waves' origin points.

This intraseasonal variance influences atmospheric moisture patterns and the propagation of intraseasonal atmospheric oscillations (DeMott et al. 2024; Chrisler and Stachnik 2023). It also represents the variability of intraseasonal tropical waves (Keshav and Landu 2020), which may be influenced by oceanic interactions such as sea surface temperature (SST) and ENSO, as they play a crucial role in the variability of intraseasonal tropical waves, including Kelvin, Rossby, TD (tropical depression waves) and MJO (Keshav and Landu 2022; Webber et al. 2010). The detection of this variability has also provided the basis for the simulation of intraseasonal oscillations in general circulation models (GCMs) (Liu et al. 2015), improving the predictability of global teleconnections associated with the intraseasonal variability of different oscillations (Straus et al. 2023).

3.3 | Annual Cycle of Waves Activity and Associated Precipitation

Figure 4 shows the activity of oscillations based on the total number of events (wet+dry) for each type of intraseasonal wave over the regions depicted in Figure 3b–e during the 1981–2022 period. In general, the TEWs events show their activity from May to December, with the highest activity occurring during the boreal summer (July–August). These results are consistent with previous studies, which state that the number of TEWs in the northern hemisphere peaks between July and September (JAS) (Russell et al. 2017; Dominguez et al. 2020; Hollis, Stachnik, et al. 2024; Hollis, McCrary, et al. 2024). KWs exhibit peak activity during April and May, with an average of five events per month. This agrees with Rakhman et al. (2017), who found that KWs are detected in symmetrical components across seasons and under all ENSO conditions. They also noted that a strong KW signal occurs from DJF to MAM, with the strongest activity during MAM. Additionally, these findings align with Wheeler and Kiladis (1999), who identified equatorial planetary wave activity in the Southern Hemisphere summer (November–April) and the Northern Hemisphere summer (May–October).

MRGs exhibit an unimodal annual cycle with peak activity from May to October and lowest activity from November to April, consistent with the peak activity reported by Roundy and Frank (2004) during the boreal summer. These results corroborate findings by Shreya and Suhas (2024), which indicate that most westward-propagating MRG wave events in the

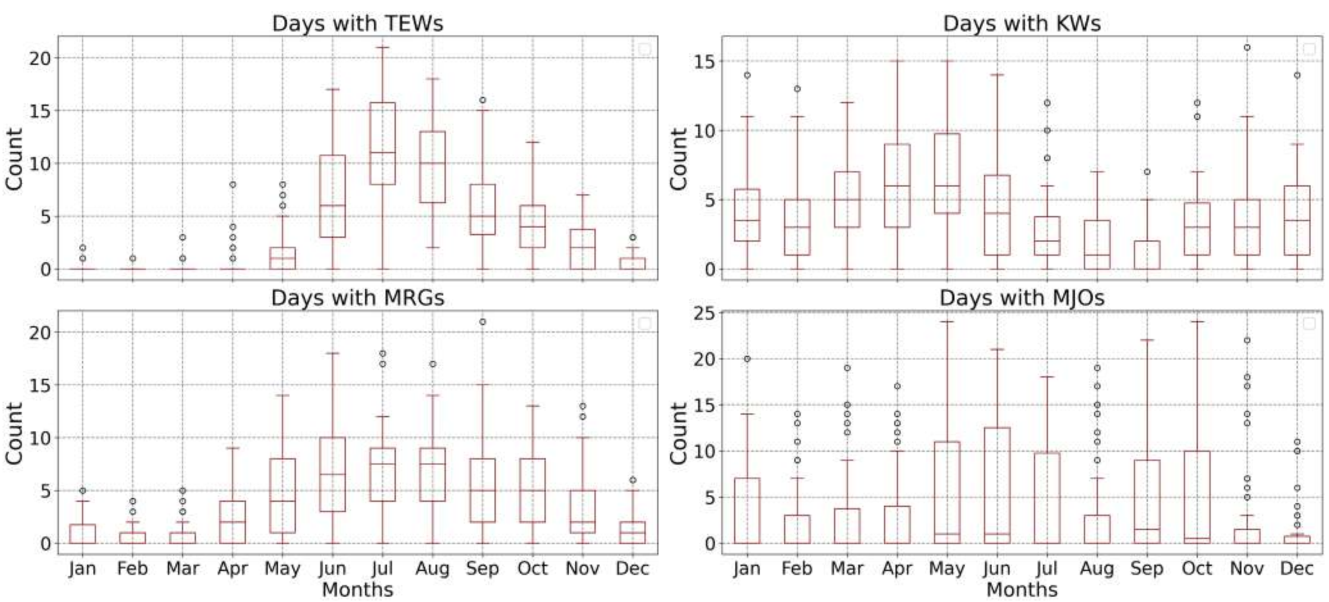

FIGURE 4 | Activity of oscillations based on the number of wet + dry events along the year associated with Tropical Easterly Waves (TEWs), Kelvin waves (KWs), Mixed Rossby-Gravity (MRGs) and Madden–Julian oscillations (MJOs). Box-plots represent the variation in the distribution of the number of wave events for each month during the years of analysis. Dots represent atypical values while the horizontal lines within the box denote the median. [Colour figure can be viewed at wileyonlinelibrary.com]

upper troposphere occur from May to October. They also reveal clear seasonality in amplitude, wavenumber, and trapping scale, suggesting a distinct peak season. Moreover, 61% of the MRG events identified by Shreya and Suhas (2024) occurred during May–October, with 65% observed over the central–east Pacific and Atlantic Ocean regions. Regarding MJOs, the highest activity occurs from May to July and September to October. However, previous studies have indicated that the tropical MJO is more active during the boreal winter and relatively weak during the boreal summer (Lu and Hsu 2017). Specifically, this work found that MJO events exhibit higher activity, stronger intensity, and longer duration during the boreal winter (Dec.–Feb.) and spring (Mar.–May). Although there is evidence of MJOs influencing precipitation in the study region (Recalde-Coronel et al. 2020), there is no consensus on their seasonality.

Figure 5 shows the percentage of total precipitation during the 1981–2022 period associated with wet and dry wave phases identified using the SEOF12 OLR index. This figure indicates that TEWs account for 30% to 40% of precipitation over northwestern Mexico, Central America, Venezuela, the eastern Pacific Ocean between 5° N and 20° N, and the tropical Atlantic around 10° N–15° N and 70°W–50° W. For KWs, the highest percentage of precipitation is found in the northern Amazon (12%–18%), the Pacific coasts of northern Peru (up to 40%), and the tropical Pacific (5° N-3° S / 100° W-120° W). MRGs show higher precipitation percentages over the Baja California peninsula (approximately 40%), western Mexico, the Pacific coasts of Central America, northern South America, and central Venezuela. The MJO accounts for approximately 10% to 12% of precipitation across all continental regions.

Overall, TEWs and MRGs contribute most to the precipitation activity in the study region, while KWs are more representative over the Amazon basin. It is important to note that each wave is active in different seasons throughout the year (Figure 4), which can lead to overlapping precipitation events. However, the isolated influence of these waves does not explain most of the region's precipitation, which is heavily influenced by seasonal and annual variability components. Similar results were found using the CHIRPS dataset (Figures S1–S3). Additionally, differences in the number of events detected may be associated with the selection method, which is based on the maximum and minimum values of the OLR index as explained in Section 2.3.

Previous results agree with the regression analysis proposed in Section 2.3 (Figure S4). For the TEWs (with an activity region 40° W–50° W;5° N–10° N), there is a positive correlation between the index and precipitation over the tropical Atlantic offshore Venezuela, the plains between the Andes and the Guiana Shield, Peru, northeastern Brazil, southern Mexico, Guatemala, Belize, and Honduras, while a negative correlation predominates in the Caribbean, northern Colombia, Panama, and Costa Rica. For KWs, with an activity region of 100° W–120° W; 2° N–10° N over the Tropical Pacific, there is a positive correlation in northern South America, including northern/central Amazonia, and a negative correlation with the precipitation in Mexico and the Pacific coasts of southern Colombia and northern Ecuador. For MRGs, with an activity region of 100° W–118° W; 5° N–8° N over the tropical Pacific, there is a positive correlation with precipitation in northern South America, Panama, Costa Rica (offshore the Pacific Ocean), and a negative band of correlation over the Pacific

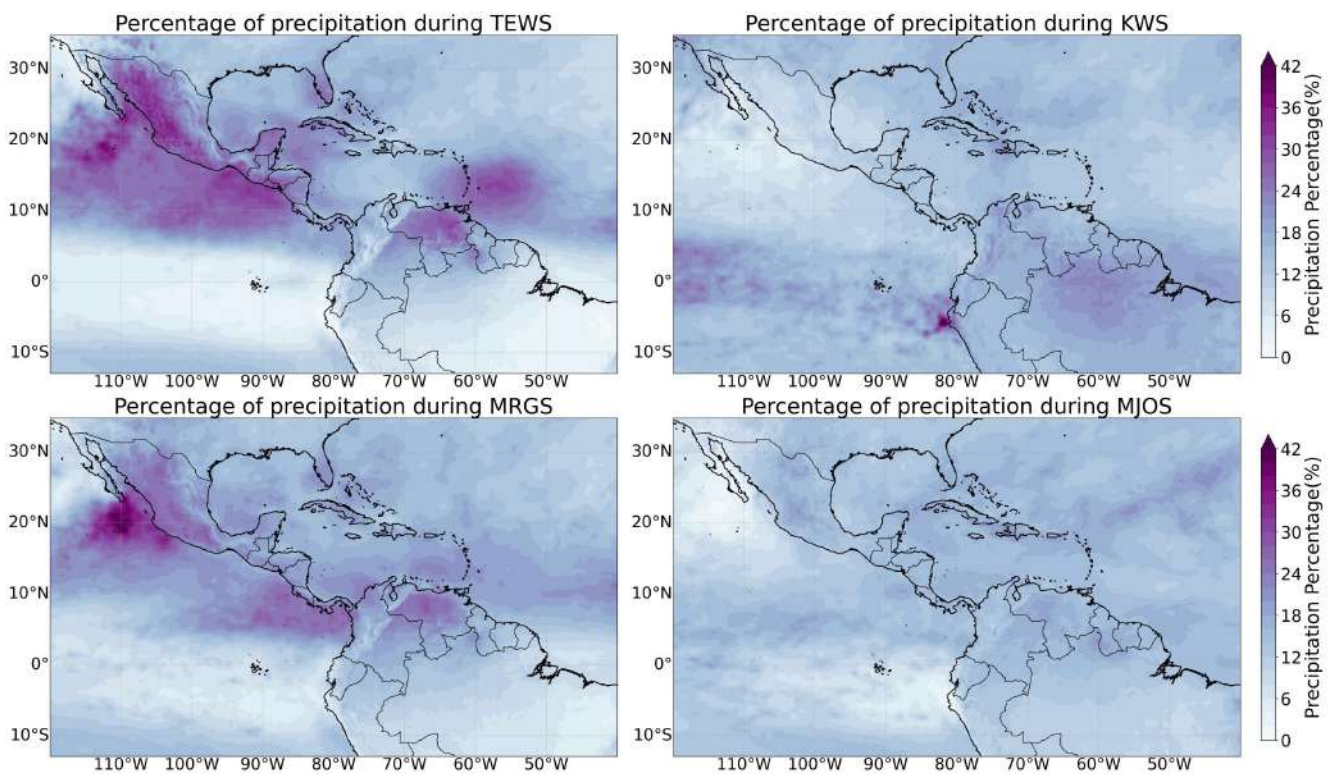

FIGURE 5 | Percentage of precipitation during episodes of TEWs, KWs, MRGs and MJOs. [Colour figure can be viewed at wileyonlinelibrary.com]

Ocean around 5° N–12° N facing Central America. For MJO, with an activity region 110° W–120° W; 8° N–12° N over the tropical Pacific, a negative correlation predominates between the MJOs and precipitation, although some regions over the Atlantic and Pacific Oceans exhibit positive correlation.

Hereafter, based on the SEOF2 OLR index, we estimate composite fields of precipitation anomalies, wind speed anomalies at 850 hPa, VIMD, and vertical integral of eastward and northward water vapour flux to aim to understand the circulation associated with the dry and wet events for each wave-type examined in the next section.

3.4 | Composites for TEWs

Figure 6 (upper row) shows the composite anomalies of precipitation during wet and dry days according to the OLR index at TEWs time scales over the region defined in Figure 3b. Across northern South America and Central America, a wave-like pattern of alternating positive and negative precipitation anomalies is evident, consistent with wind speed anomalies at 850 hPa and VIMD. During wet days, regions with positive precipitation anomalies agree with areas of negative VIMD (convergence), and vice versa during dry days. The VIWVF highlights water vapour pathways associated with these conditions.

On wet days, positive precipitation anomalies are observed over the Caribbean Sea, the Pacific coast of Central America, and a region in the tropical Atlantic between 40° W–55° W and 5° N–15° N. Convergence zones appear over the Panama Bay and the Guianas, driven by winds from the Pacific, Caribbean and Amazon regions. Conversely, dry conditions prevail along the eastern Andes and the eastern Pacific coast of Guatemala. During dry days, negative precipitation anomalies are found over the Atlantic Ocean and the Caribbean coasts of Colombia and Panama, while positive anomalies occur over Venezuela, eastern Colombia, and parts of the North Atlantic. Notably, a

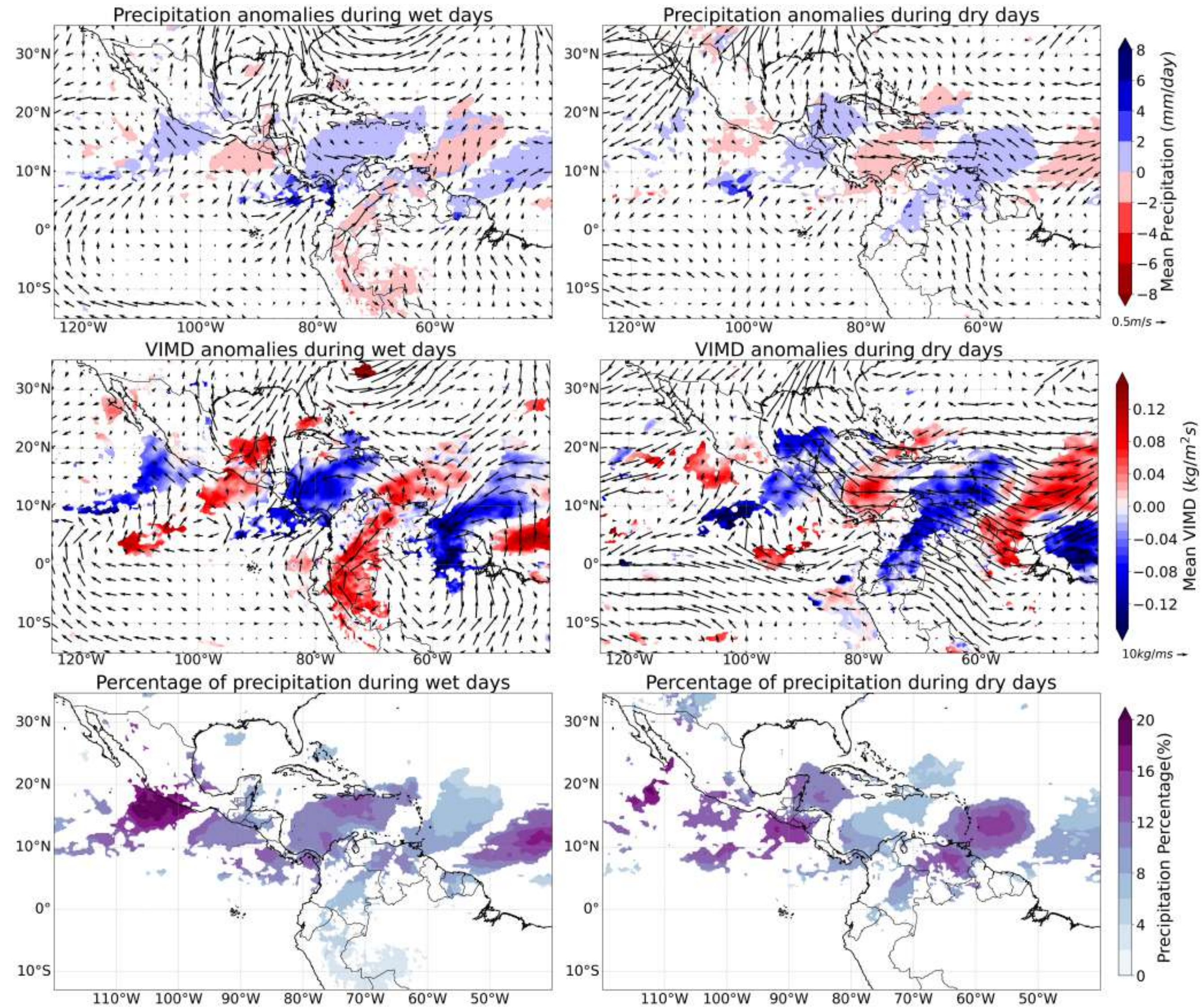

FIGURE 6 | Composites of precipitation anomalies (top row), vertically integrated moisture divergence anomalies (middle row) and percentage of precipitation during wet and dry episodes (bottom row) associated with TEWs. Coloured areas represent composite values with statistical significance at the 0.95 confidence level. Wind speed anomalies at 850 hPa are shown in the top row, and vertically integrated moisture transport vectors are displayed for wet and dry episodes in the middle row. [Colour figure can be viewed at wileyonlinelibrary.com]

wave-like trough is observed over northern South America and the Caribbean Sea.

Valencia et al. (2024) reported similar findings during the OTREC campaign, noting enhanced precipitation during wet TEW days due to intensified cross-equatorial flow and a stronger meridional ChocoJet. In contrast, dry TEW days were associated with a stronger Caribbean low-level jet (CLLJ) and a weaker ChocoJet. Our results agree with these observations, suggesting that a stronger CLLJ may be linked to dry TEWs, although further research is needed. Moreover, previous studies have linked the cyclonic circulation of TEWs to an increase in the CLLJ at 850 hPa (Molinari and Vollaro 2000; Serra et al. 2010). Our analysis shows that during wet days, VIWVF from the Pacific to the Caribbean, along with negative VIMD, supports enhanced precipitation, while during dry days, positive VIMD (divergence) does not organise precipitation similarly. We hypothesise that wet days benefit from stabilised wind shear due to the ChocoJet, promoting convection, whereas an enhanced CLLJ favours destabilisation during dry days.

Figure 7 (bottom row) indicates that TEWs account for around 20% of precipitation in the central Pacific coast of Mexico, more than 16% in the Caribbean, 12% in Southern Mexico, the Pacific coast of Central America, Guatemala, El Salvador and central Venezuela, potentially contributing up to 30% combined. Despite methodological differences, our findings are consistent with previous studies by Hollis, Stachnik, et al. (2024) and Dominguez et al. (2020).

3.5 | Composites for Kelvin Waves

Figure 7 (upper row) shows the composite anomalies of precipitation during the wet and dry days according to OLR over the region defined in Figure 3c. During dry days, the eastern Pacific around 10° N, between 100° W and 120° W, exhibits negative anomalies (indicating dry conditions), with strong patches around 8° N, 92° W and the southern Colombian Pacific (2° N, 78° W). In contrast, positive precipitation anomalies (indicating wet conditions) are observed over large parts of Northern South America including the northern Amazon,

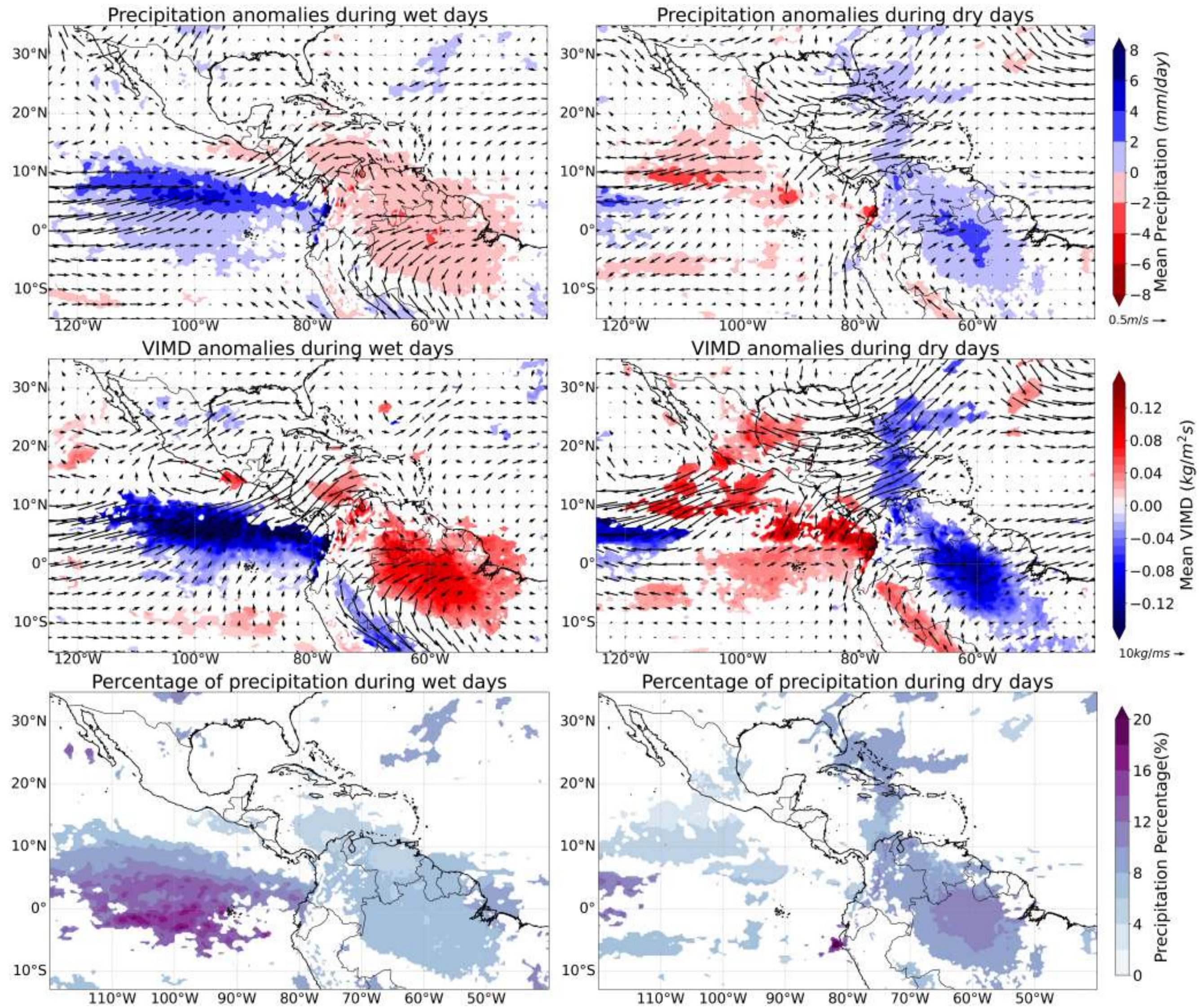

FIGURE 7 | Same as Figure 6 for KWs. [Colour figure can be viewed at wileyonlinelibrary.com]

Orinoco region, eastern and central Colombia, with anomalies extending over portions of the Caribbean Sea. The regions of wet (dry) conditions over northern South America correspond well with the areas of moisture convergence (divergence) (Figure 7) and the low-level wind anomalies (850 hPa) converging towards wet regions and diverging from the dry regions.

During wet days, a strong dipole is observed between the eastern Pacific Ocean and Northern South America: positive precipitation anomalies in the former and negative anomalies in the latter region. The figure also shows that in the eastern Pacific, a region of wet conditions, low-level winds (at 850 hPa) converge, while over the Amazon, winds diverge into two branches: one flows southward, and the other reaches the Caribbean Sea before joining the Pacific Ocean (Figure 7). Notably, opposite anomalies are seen during dry and wet events in the regions of high variance for KW: the Amazon and the eastern Pacific. Liebmann et al. (2009) and Mayta et al. (2021) suggest that KWs originating from the Pacific and South America have different characteristics; the latter shows strong signals of wave trains at upper levels. In this study, we only consider the waves with Pacific precursors, and our results suggest that wet (dry) events over the Pacific coincide with dry (wet) events in the Amazon.

Figure 7 presents the percentage of precipitation associated with KWs during wet and dry days. The highest percentages (up to 20% combined) are found in the Amazon and Orinoco River basins (eastern Colombia, western Venezuela and northern Brazil), while during wet days, the highest percentages are observed in the tropical eastern Pacific. This result highlights the importance of KWs in Northern South America's hydroclimate, as they account for up to 20% of the precipitation in portions of the two greatest basins in the region (Figure 5 and Figure S3).

3.6 | Composites for MRG Waves

Figure 8 (upper row) shows the composite anomalies of precipitation during the wet and dry days according to the OLR index at MRG time scales over the region defined in Figure 3d. During both wet and dry days, a dipole pattern is evident, indicating the

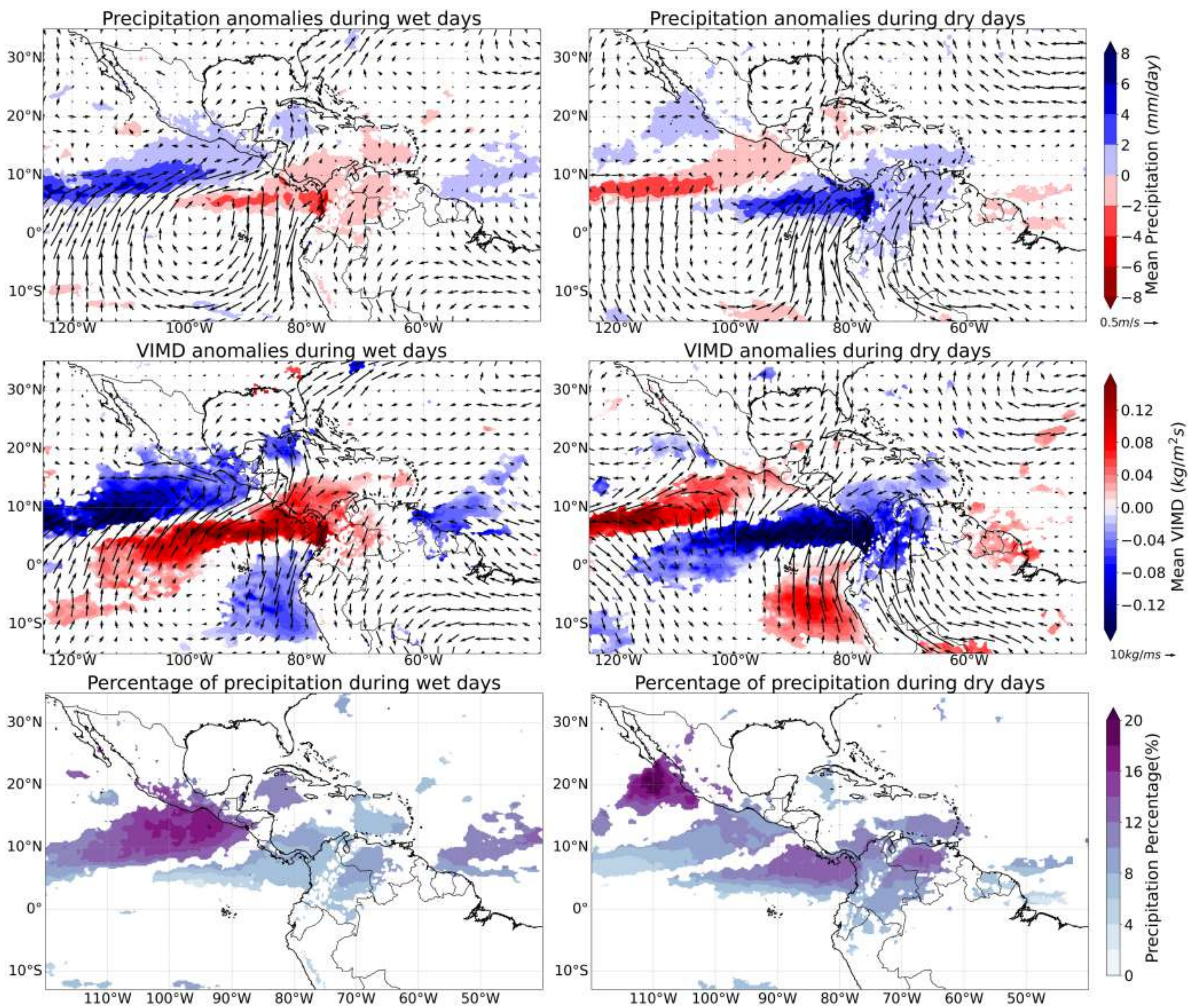

FIGURE 8 | Same as Figure 6 for MRGs. [Colour figure can be viewed at wileyonlinelibrary.com]

westward propagating signal of these MRGs originating in the central-east Pacific, as described by Shreya and Suhas (2024). On wet days, positive anomalies (indicating wet conditions) dominate over the eastern Pacific (around 10° N), while negative anomalies (indicating dry conditions) extend across the Panama gap and the Colombian Pacific Ocean, reaching as far as 100° W. These spatial patterns are consistent with those shown in the VIMD (Figure 8, middle row), where regions with positive (negative) anomalies of precipitation correspond to areas with positive (negative) VIMD. Similarly, regions with positive anomalies (in both precipitation and VIMD) are linked to areas of convergence, while regions with negative anomalies are associated with divergence areas. Notably, the anticyclonic circulation over the eastern Pacific is characterised by winds flowing from a region of divergence (the Panama gap) into a convergence area (the eastern Pacific around 100° W).

During dry days, we observed patterns opposite to those on wet days. Negative precipitation anomalies (indicating dry conditions) prevail over the Pacific Ocean between 100° W and 120° W around 8° N, while positive anomalies (indicating wet conditions) dominate over the Colombian Pacific Ocean, extending as far as 100° W. Interestingly, the Colombian Pacific Ocean appears as a convergence area, with winds coming from divergent and dry regions of the Peruvian coast and the eastern Pacific around 10° N. It is important to note the possible modulation of the cross-equatorial flow via the Orinoco Low-Level Jet (OLLJ) over the MRG. We hypothesise that during wet days, northerly winds (from the tropical Atlantic Ocean) remain active along the OLLJ corridor, while during dry days, southerly winds (from the Amazon) prevail along the OLLJ pathway. To our knowledge, this is the first time that the relationship between the OLLJ and the MRG has been highlighted, and it warrants further research.

Additionally, Figure 8 (bottom row) presents the percentage of precipitation accounted for by MRGs during dry and wet days. During wet days, the highest percentages are found in southwestern Mexico and the eastern Pacific Ocean between 8° N and 15° N, eastern and western Colombia, and both Pacific and Caribbean in NSA (up to 8%). During dry days, areas of high precipitation include the Pacific coast of Central America, eastern Pacific, Colombia and central Venezuela, and nearly 20% of the precipitation over the Gulf of California. Horinouchi (2013) suggests that MRGs are highly anti-correlated with precipitation over the tropical western to Central Pacific Ocean during boreal summer and that there is no year-round effect of these oscillations over precipitation, while on the other hand, we found that there is a clear correlation between MRGs and precipitation in the eastern Pacific, enhancing our understanding of the regional distinct impact of MRGs in the Pacific region. In this context, when the MRG generates positive anomalies in OLR, we observe higher precipitation over the region. However, according to Fahrin et al. (2024), these percentages should be interpreted with caution due to the broad spectral band of MRGs and its relationship with the position of the Intertropical Convergence Zone in the region.

3.7 | Composites for MJO

Figure 9 (upper row) shows the significant precipitation anomalies during wet and dry days according to the OLR index developed at MJO time scales. Notably, wet (dry) days correspond to positive (negative) precipitation anomalies centred over the Eastern North Pacific Ocean (ENP). This oceanic pattern also connects to continental regions from southern Mexico to Colombia (from 20° N, 0° N). The positive precipitation anomalies associated with wet days are higher and more extensive than the negative anomalies during dry days. During wet days, anomalies of up to +6 mm/day reach the Caribbean coasts of Mexico, Central America, northern and western Colombia, and even some regions of the Orinoco and Amazon River basins. During dry days, anomalies of up to −2 mm/day remain significant over Central America and northern Colombia without reaching the Caribbean Sea.

These significant patterns of positive (negative) precipitation anomalies correspond to strong convergence (divergence) of atmospheric moisture flux over the ENP, continental Central America, and western/northern Colombia (Figure 9 middle row). Anomaly vectors of VIWVF also reveal that during wet (dry) days, the ENP acts as a sink (source) of atmospheric moisture coming from (going to) the tropical central Pacific (5° S–15° N). Finally, Figure 9 (bottom row) presents the percentage of precipitation accounted for by MJOs during wet and dry days. Consistent with the results on precipitation and VIMD, wet days concentrate a higher percentage of precipitation than dry days. During wet days, the highest percentage of precipitation is centred over the ENP, from 15° N to 20° N off the coasts of southern Mexico and Guatemala (reaching up to 20%), as well as over eastern Mexico, the Caribbean and Central America (around 15%), and western Colombia (up to 10%). During dry days, the highest percentages of precipitation are found over the Pacific Ocean, the Gulf of Mexico, southern Mexico, the Yucatán Peninsula, Central America, the far eastern Pacific from 10° N up to 15° N, and northwestern Colombia.

Maloney and Hartmann (2000) found that during boreal summers, MJO events amplify locally over the ENP near Central America, which aligns with our findings (Figures 4 and 9). Clearly, the MJO significantly influences precipitation and atmospheric moisture flux over the ENP by modulating SST anomalies and enhancing off-equatorial convection (Maloney and Kiehl 2002). Increased convection in the ENP is driven by westerly wind anomalies, causing cyclonic low-level shear and enhancing convergence north of the maximum winds. Furthermore, convection inflow over Central America, Mexico and the western Caribbean Sea further strengthens ENP circulation, with additional topographic effects over land (Maloney and Hartmann 2000).

4 | Final Remarks and Future Work

We studied the spatiotemporal intraseasonal variability using regression coefficients, variance analysis and empirical orthogonal function spectra through daily OLR data spanning 42 years (1981–2022). Our analysis reveals that the largest contributions to OLR variability are associated with convectively coupled KWs and the MJO, with smaller contributions from TEWs and MRG waves.

Our findings present a clear wave-type structure for the TEWs over the study region, showing consistency between the wet

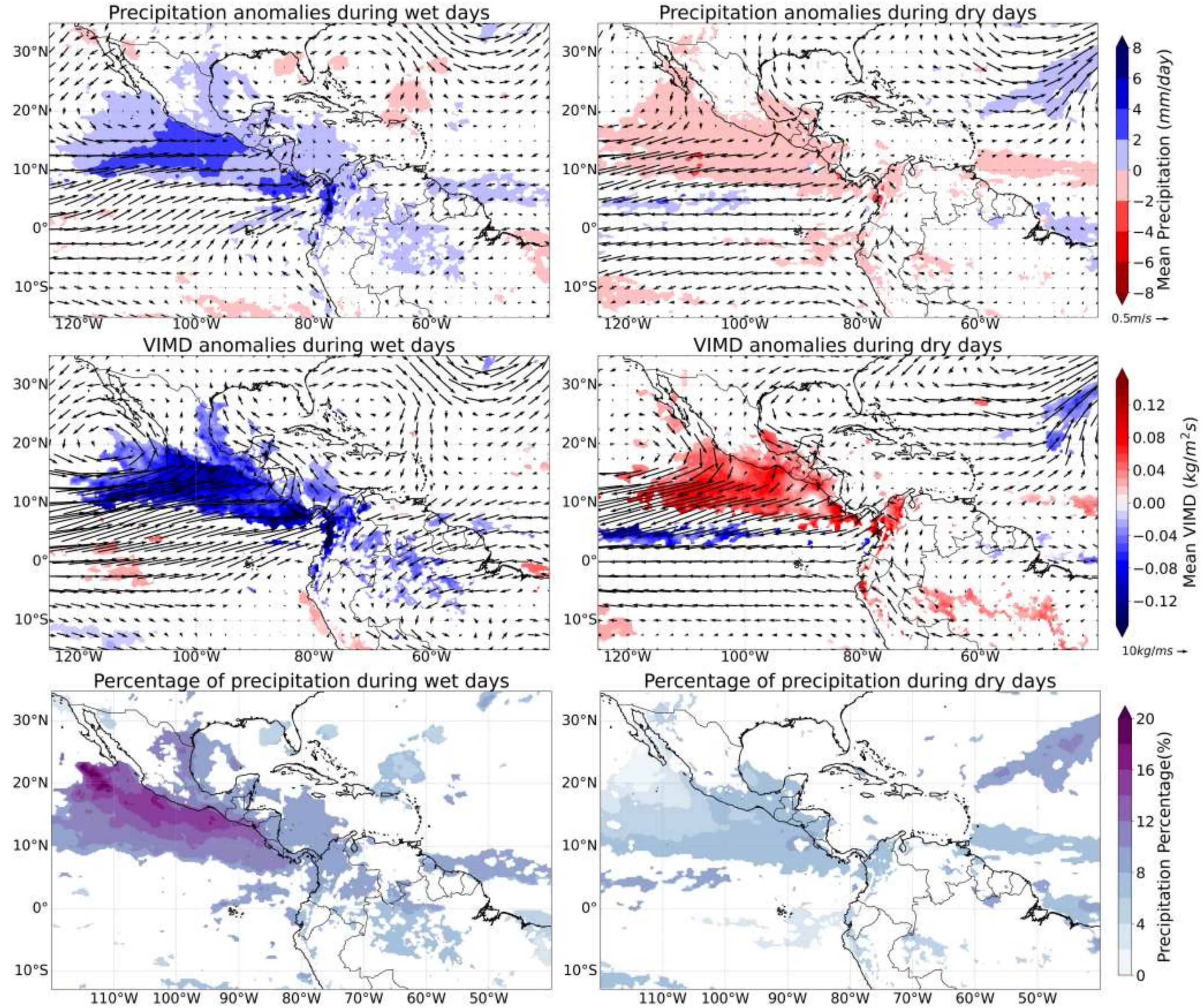

FIGURE 9 | Same as Figure 6 for MJOs. [Colour figure can be viewed at wileyonlinelibrary.com]

(dry) events classification based on the OLR index and moisture convergence (divergence). Furthermore, these patterns reveal interesting coherence with water vapour sources and low-level interactions over the study region. Notably, during wet days, two areas of convergence were identified: the Panama Bay and the Guianas. It is important to note that the TEW events can be associated with an increase in precipitation of up to ~20% in some locations. Specifically, wet TEW days coincide with an increase in precipitation (compared to days without TEWs) by 15%–20% over the tropical Atlantic, the Caribbean Sea, the far-eastern Pacific near Colombia, and the southern Pacific coast of Mexico. Conversely, dry TEW days also exhibit an increase in precipitation of around 10%–15% but in different locations, such as the northeastern Atlantic coast and continental Venezuela, as well as the southern coasts of Nicaragua, El Salvador, and Guatemala. Interestingly, the eastern Pacific emerges as an area of significant precipitation contribution during both dry and wet events.

For Kelvin waves, a notable dipole of precipitation anomalies during wet days is observed between the eastern Pacific (positive anomalies) and northern South America (negative anomalies). The opposite pattern occurs during dry days. This dipole aligns with two sources of Kelvin waves identified in the region: the eastern Pacific and the Amazon (Liebmann et al. 2009). During wet (dry) days, precipitation exhibits significant positive (negative) anomalies over the Amazon and northeastern South America. Most of these patterns can be associated with regions of low-level wind convergence (divergence) or VIMD. However, some regions experiencing significant hydroclimatic changes, like the Caribbean and Mexico, cannot be explained solely by these variables. In general, Kelvin waves can be associated with a precipitation increase of around 15% over the far-eastern Pacific Ocean during wet days, while precipitation increases by around 10% over the Amazon, eastern Colombia, Venezuela, the Caribbean islands and the Central Pacific.

For MRGs, we identified what appears to be an oscillation-like pattern travelling from the Central Pacific, as noted by Suhas et al. (2020). This MRG wave-like pattern exhibits a dipole over the eastern Pacific around 10° N. An interesting moisture pathway exists between the Colombian Pacific (reaching 90° W) and the eastern Pacific (100° W-120° W, 10° N), with the latter region acting as a convergence area during wet MRG days, while the opposite occurs during dry days. Unlike TEWs and KWs, MRGs colocate their precipitation regions in correspondence with the convergence areas and precipitation anomalies. During wet days, the highest contribution of precipitation is observed over the southwestern Pacific coast of Mexico, accounting for up to 20%. This study provides novel findings regarding the influence of MRGs on the hydroclimate of Southern North America, Central America and Northern South America.

For MJOs, we found that precipitation anomalies are centred over the Eastern North Pacific, being positive (negative) for the wet (dry) MJO days. This result agrees with previous studies that have demonstrated the influence of MJOs in modulating the precipitation in Mexico and Central America (Barlow and Salstein 2006; Perdigón-Morales et al. 2019, 2021). During wet days, we observed higher convergence and precipitation along the Pacific Ocean coasts from northern Ecuador to central Mexico. During wet MJO days, the highest contribution to precipitation is observed over the ENP region and the coasts of southern Mexico and Guatemala, corresponding to up to 16%.

TEWs and MRGs are highlighted as important sources of precipitation in three particular regions: Mexico, Central America and Venezuela. These regions not only contain the majority of the population within the study area but also encompass basins of great ecohydrological relevance, such as the Orinoco, Northern Amazon and the Usumacinta basins. For tropical basins, there are processes of great importance, such as the recycling of atmospheric moisture within the 3 to 20-day timescales (van der Ent and Savenije 2011; Zemp et al. 2014; Enciso et al. 2022), which can be strongly influenced by intraseasonal oscillations and maintain the stability of the water cycle and the tropical ecosystems (Zemp et al. 2017; Beveridge et al. 2024). Then, our findings related to MRGs present new insights into how these oscillatory processes influence long-term precipitation.

Figure 10 presents a schematic representation of the areas within the study region where there are positive or negative precipitation anomalies during the wet and dry days defined with the SEOF12 OLR index. This figure gives us a general glance over the possible interaction between oscillatory processes in the study region in this long-term analysis and opens new research avenues regarding the quantification of the temporal and spatial interaction of these processes over the year or the study period.

This study raises new questions for future research such as follows: (i) Are rainfall extremes in the region related to the intraseasonal oscillation activity?; (ii) What is the influence of each intraseasonal wave type on the streamflows?; (iii) How are oceanic circulation patterns, precipitation anomalies, and sea surface temperatures related during the active phases of each oscillation?; (iv) Is there synchronisation between intraseasonal oscillations that might influence precipitation

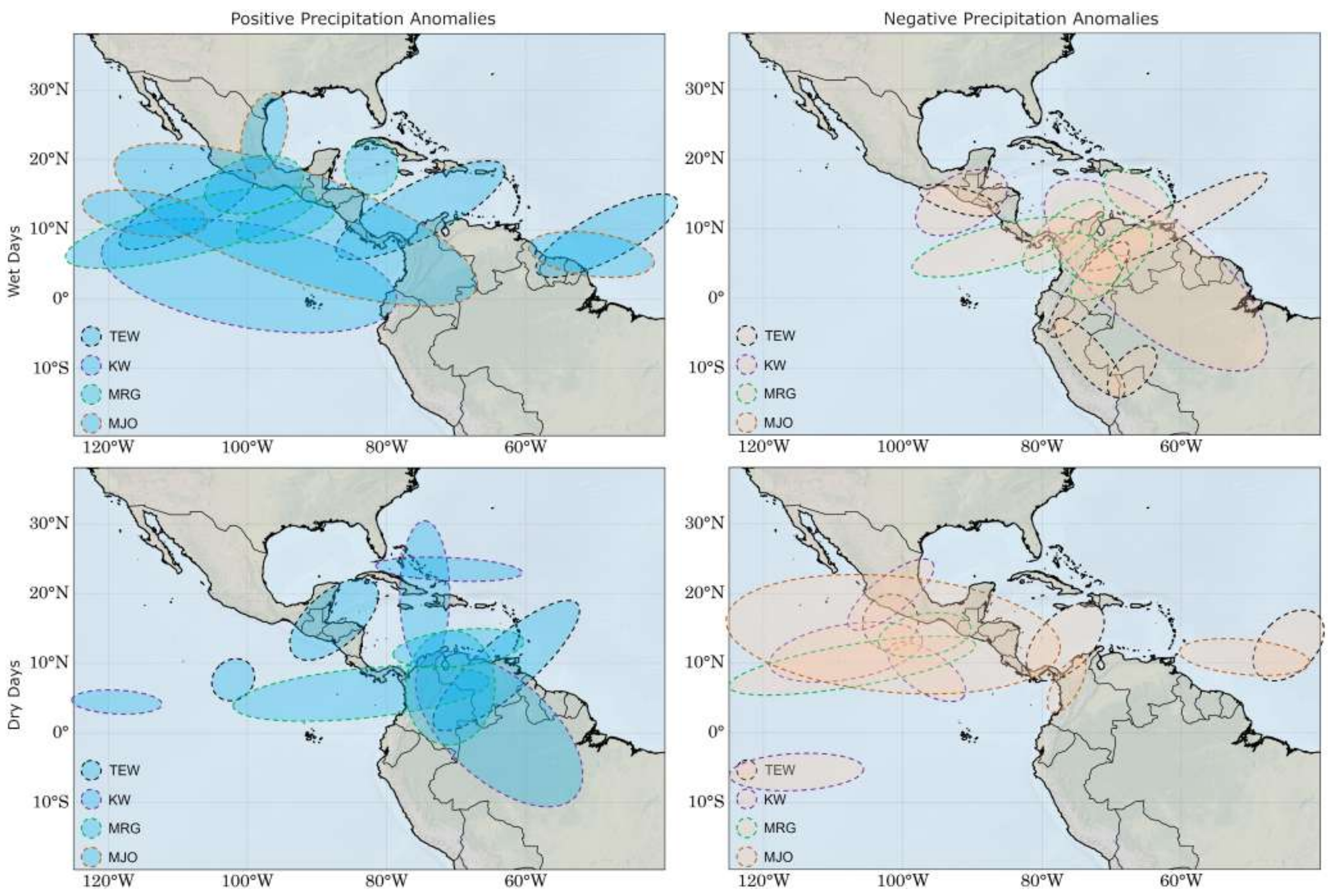

FIGURE 10 | Schematic representation of the intraseasonal oscillations interaction when there is a positive or negative precipitation anomaly in the region during wet and dry days. [Colour figure can be viewed at wileyonlinelibrary.com]

patterns over the region?; (v) How is the spatial interaction of intraseasonal oscillations, revealed with local indices, over other tropical regions such as the Indian Ocean and Australia?; (vi) How is the role of the Tropical Pacific EWs in the modulation of precipitation over Northern South America, Central America and Mexico?

Author Contributions

Alejandro Builes-Jaramillo: conceptualization, methodology, formal analysis, software, funding acquisition, investigation, writing – original draft, writing – review and editing, resources, supervision, data curation, visualization. **Johanna Yepes:** project administration, conceptualization, methodology, funding acquisition, writing – original draft, writing – review and editing, software, formal analysis, investigation, visualization. **Hernán D. Salas:** conceptualization, methodology, formal analysis, investigation, writing – original draft, writing – review and editing, visualization, validation. **Juan M. Bedoya-Soto:** formal analysis, writing – review and editing, writing – original draft. **Paris Rivera:** formal analysis, writing – review and editing, writing – original draft. **Juliana Valencia:** formal analysis, writing – review and editing, writing – original draft. **Alejandra M. Carmona:** formal analysis, writing – review and editing, writing – original draft.

Acknowledgements

The work of A. Builes-Jaramillo and J. Yepes is supported by the Institución Universitaria Colegio Mayor de Antioquia (project FAI149). The work by H.D. Salas is supported by the Instituto Tecnológico Metropolitano. Authors thank Dr. Alejandro Jaramillo, Dra. Christian Domínguez Sarmiento, and Dr. Jorge Garcia-Franco from the Instituto de Ciencias de la Atmósfera y Cambio Climático, Universidad Autónoma de México, for their useful comments in the early stage of this research. Special thanks to Dr. Alejandro Jaramillo who provided the Wave Number-Frequency Power Spectra and Fourier Filters over the ERA5 OLR datasets used in this work. Also, authors thank Carolina Florian and Sebastian Gómez from the Institución Universitaria Colegio Mayor de Antioquia. Thanks to the European Centre for Medium-Range Weather Forecast ECMWF for the ERA5 datasets. Thanks to the Climate Hazards Center UC Santa Barbara for the Climate Hazards Group InfraRed Precipitation with Station—CHIRPS.

Conflicts of Interest

The authors declare no conflicts of interest.

Data Availability Statement

The data sets used in this study are available online. ERA5 atmospheric reanalysis [Dataset] (Hersbach et al. 2019) is available at https://cds.climate.copernicus.eu/cdsapp#!/dataset/reanalysis-era5-single-levels-monthly-means. The data set Climate Hazards Group InfraRed Precipitation with Station—CHIRPS is available at https://www.chc.ucsb.edu/data/chirps.

References

Aiyyer, A. R., and J. Molinari. 2003. "Evolution of Mixed Rossby–Gravity Waves in Idealized Mjo Environments." *Journal of the Atmospheric Sciences* 60: 2837–2855. https://journals.ametsoc.org/view/journals/atsc/60/23/1520-0469_2003_060_2837_eomrwi_2.0.co_2.xml.

Alvarez, M. S., C. Vera, G. Kiladis, and B. Liebmann. 2016. "Influence of the Madden Julian Oscillation on Precipitation and Surface Air Temperature in South America." *Climate Dynamics* 46: 245–262. https://www.scopus.com/inward/record.uri?eid=2-s2.0-8495573945410.1007.

Barlow, M., and D. Salstein. 2006. "Summertime Influence of the Madden-Julian Oscillation on Daily Rainfall Over Mexico and Central America." *Geophysical Research Letters* 33: L21708.

Berry, G. J., and C. Thorncroft. 2005. "Case Study of an Intense African Easterly Wave." *Monthly Weather Review* 133: 752–766.

Beveridge, C. F., J.-C. Espinoza, S. Athayde, et al. 2024. "The Andes–Amazon–Atlantic Pathway: A Foundational Hydroclimate System for Social–Ecological System Sustainability." *Proceedings of the National Academy of Sciences* 121, no. 22: e2306229121. https://doi.org/10.1073/pnas.2306229121.

Cárdenas, S. G., P. A. Arias, and S. C. Vieira. 2017. "The African Easterly Waves Over Northern South America." *Proceedings* 1: 165.

Cattell, R. B. 1966. "The Scree Test for the Number of Factors." *Multivariate Behavioral Research* 1: 245–276. https://doi.org/10.1207/s15327906mbr0102_10.

Chen, B., W. Wen Tung, and M. Yanai. 2016. "Multiscale Temporal Mean Features of Perturbation Kinetic Energy and Its Budget in the Tropics: Review and Computation." *Meteorological Monographs* 56: 8.1–8.23. https://journals.ametsoc.org/view/journals/amsm/56/1/amsmonographs-d-15-0017.1.xml.

Chien, M.-T., and D. Kim. 2023. "Representation of the Convectively Coupled Kelvin Waves in Modern Reanalysis Products." *Journal of the Atmospheric Sciences* 80: 397–418.

Chrisler, B., and J. P. Stachnik. 2023. "Tropical-Wave Activity and Madden–Julian Oscillation Termination." *Quarterly Journal of the Royal Meteorological Society* 149: 61–83. https://doi.org/10.1002/qj.4393.

Cornforth, R., Z. Mumba, D. J. Parker, et al. 2017. *Synoptic Systems*, 40–89. Wiley.

das Chagas Vasconcelos Junior, F., C. Jones, A. W. Gandu, and E. S. P. R. Martins. 2021. "Impacts of the Madden-Julian Oscillation on the Intensity and Spatial Extent of Heavy Precipitation Events in Northern Northeast Brazil." *International Journal of Climatology* 41: 3628–3639.

DeMott, C. A., J. H. Ruppert, and A. Rydbeck. 2024. "Intraseasonal Variability in the Indian Ocean Region." In *The Indian Ocean and Its Role in the Global Climate System*, 79–101. Elsevier. https://linkinghub.elsevier.com/retrieve/pii/B9780128226988000068.

Dias, J., S. Leroux, S. N. Tulich, and G. N. Kiladis. 2013. "How Systematic Is Organized Tropical Convection Within the Mjo?" *Geophysical Research Letters* 40: 1420–1425. https://doi.org/10.1002/grl.50308.

Dominguez, C., J. M. Done, and C. L. Bruyère. 2020. "Easterly Wave Contributions to Seasonal Rainfall Over the Tropical Americas in Observations and a Regional Climate Model." *Climate Dynamics* 54: 191–209. https://doi.org/10.1007/s00382-019-04996-7.

Enciso, A. M., O. L. Baquero, D. Escobar-Carbonari, J. Tapasco, and W. L. Cerón. 2022. "Variability of Precipitation Recycling and Moisture Sources Over the Colombian Pacific Region: A Precipitationshed Approach." *Atmosphere* 13: 1202.

Fahrin, F., A. O. Gonzalez, B. Chrisler, and J. P. Stachnik. 2024. "The Relationship Between Convectively Coupled Waves and the East Pacific Itcz." *Journal of Climate* 37: 2565–2583. https://journals.ametsoc.org/view/journals/clim/37/8/JCLI-D-23-0398.1.xml.

Fathullah, N. Z., S. W. Lubis, and S. Setiawan. 2017. "Characteristics of Kelvin Waves and Mixed Rossby-Gravity Waves in Opposite Qbo Phases." *IOP Conference Series: Earth and Environmental Science* 54: 012032. https://www.scopus.com/inward/record.uri?eid=2-s2.0-8501493109910.1088.

Feng, T., X.-Q. Yang, W. Zhou, R. Huang, L. Wu, and D. Yang. 2016. "Synoptic-Scale Waves in Sheared Background Flow Over the Western North Pacific." *Journal of the Atmospheric Sciences* 73: 4583–4603. https://journals.ametsoc.org/view/journals/atsc/73/11/jas-d-16-0064.1.xml.

Feng, X., G. Y. Yang, K. I. Hodges, and J. Methven. 2023. "Equatorial Waves as Useful Precursors to Tropical Cyclone Occurrence and Intensification." *Nature Communications* 14: 1–11.

Ferrett, S., G.-Y. Yang, S. J. Woolnough, J. Methven, K. Hodges, and C. E. Holloway. 2020. "Linking Extreme Precipitation in Southeast Asia to Equatorial Waves." *Quarterly Journal of the Royal Meteorological Society* 146: 665–684. https://doi.org/10.1002/qj.3699.

Fink, A. H., and A. Reiner. 2003. "Spatiotemporal Variability of the Relation Between African Easterly Waves and West African Squall Lines in 1998 and 1999." *Journal of Geophysical Research: Atmospheres* 108: 4332.

Fung, I. Y., D. E. Harrison, and A. A. Lacis. 1984. "On the Variability of the Net Longwave Radiation at the Ocean Surface." *Reviews of Geophysics* 22: 177–193. https://doi.org/10.1029/RG022i002p00177.

Funk, C., P. Peterson, M. Landsfeld, et al. 2015. "The Climate Hazards Infrared Precipitation With Stations—A New Environmental Record for Monitoring Extremes." *Scientific Data* 2: 150066. http://www.nature.com/articles/sdata201566.

Gelbrecht, M., N. Boers, and J. Kurths. 2018. "Phase Coherence Between Precipitation in South America and Rossby Waves." *Science Advances* 4, no. 12: eaau3191. https://doi.org/10.1126/sciadv.aau3191.

Grimm, A. M. 2019. "Madden–Julian Oscillation Impacts on South American Summer Monsoon Season: Precipitation Anomalies, Extreme Events, Teleconnections, and Role in the Mjo Cycle." *Climate Dynamics* 53: 907–932.

Gu, G., R. F. Adler, G. J. Huffman, and S. Curtis. 2004. "African Easterly Waves and Their Association With Precipitation." *Journal of Geophysical Research: Atmospheres* 109: D04101.

Guo, Y., X. Jiang, and D. E. Waliser. 2014. "Modulation of the Convectively Coupled Kelvin Waves Over South America and the Tropical Atlantic Ocean in Association With the Madden–Julian Oscillation." *Journal of the Atmospheric Sciences* 71: 1371–1388. https://journals.ametsoc.org/view/journals/atsc/71/4/jas-d-13-0215.1.xml.

Hendon, H. H., and B. Liebmann. 1991. "The Structure and Annual Variation of Antisymmetric Fluctuations of Tropical Convection and Their Association With Rossby–Gravity Waves." *Journal of Atmospheric Sciences* 48: 2127–2140. https://journals.ametsoc.org/view/journals/atsc/48/19/1520-0469_1991_048_2127_tsaavo_2_0_co_2.xml.

Herman, M. J., Z. Fuchs, D. J. Raymond, and P. Bechtold. 2016. "Convectively Coupled Kelvin Waves: From Linear Theory to Global Models." *Journal of the Atmospheric Sciences* 73: 407–428.

Hersbach, H., B. Bell, P. Berrisford, et al. 2019. "Global Reanalysis: Goodbye ERA-Interim, Hello ERA5." ECMWF Newsletter, 17–24.

Hollis, M. A., J. P. Stachnik, C. Lewis-Merritt, R. R. McCrary, and E. R. Martin. 2024b. "Precipitation Characteristics of Easterly Waves Across the Global Tropics." *Journal of Geophysical Research: Atmospheres* 129: e2023JD039957.

Hollis, M. A., R. R. McCrary, J. P. Stachnik, C. Lewis-Merritt, and E. R. Martin. 2024a. "A Global Climatology of Tropical Easterly Waves." *Climate Dynamics* 62: 2317–2332. https://doi.org/10.1007/s00382-023-07025-w.

Horinouchi, T. 2013. "Modulation of Seasonal Precipitation Over the Tropical Western/Central Pacific by Convectively Coupled Mixed Rossby-Gravity Waves." *Journal of the Atmospheric Sciences* 70: 600–606.

Huaman, L., C. Schumacher, and G. N. Kiladis. 2020. "Eastward-Propagating Disturbances in the Tropical Pacific." *Monthly Weather Review* 148: 3713–3728. https://journals.ametsoc.org/view/journals/mwre/148/9/mwrD200029.xml.

Lin, J., T. Qian, H. B. Bluestein, et al. 2022. "Current Challenges in Climate and Weather Research and Future Directions." *Atmosphere-Ocean* 60, no. 3-4: 506–517.

Perdigón-Morales, J., R. Romero-Centeno, P. Ordoñez, R. Nieto, L. Gimeno, and B. S. Barrett. 2021. "Influence of the Madden-Julian Oscillation on Moisture Transport by the Caribbean Low Level Jet During the Midsummer Drought in Mexico." *Atmospheric Research* 248: 105243. https://doi.org/10.1016/j.atmosres.2020.105243.

Keshav, B. S., and K. Landu. 2020. "Role of Sea Surface Temperature on the Equatorial Waves and Intraseasonal Oscillations." *Theoretical and Applied Climatology* 140: 993–1004. https://doi.org/10.1007/s00704-020-03128-0.

Keshav, B. S., and K. Landu. 2022. "Seasonality in Long-Term Trends of Tropical Intraseasonal Wave Activity." *Meteorology and Atmospheric Physics* 134: 6. https://doi.org/10.1007/s00703-021-00844-8.

Kiladis, G. N., J. Dias, and M. Gehne. 2016. "The Relationship Between Equatorial Mixed Rossby–Gravity and Eastward Inertio-Gravity Waves. Part i." *Journal of the Atmospheric Sciences* 73: 2123–2145. https://journals.ametsoc.org/view/journals/atsc/73/5/jas-d-15-0230.1.xml.

Kiladis, G. N., M. C. Wheeler, P. T. Haertel, K. H. Straub, and P. E. Roundy. 2009. "Convectively Coupled Equatorial Waves." *Reviews of Geophysics* 47: RG2003. https://doi.org/10.1029/2008RG000266.

Knippertz, P., M. Gehne, G. N. Kiladis, et al. 2022. "The Intricacies of Identifying Equatorial Waves." *Quarterly Journal of the Royal Meteorological Society* 148: 2814–2852.

Koval, A. V., O. N. Toptunova, M. A. Motsakov, et al. 2023. "Numerical Modelling of Relative Contribution of Planetary Waves to the Atmospheric Circulation." *Atmospheric Chemistry and Physics* 23: 4105–4114. https://acp.copernicus.org/articles/23/4105/2023/.

Latos, B., P. Peyrillé, T. Lefort, et al. 2023. "The Role of Tropical Waves in the Genesis of Tropical Cyclone Seroja in the Maritime Continent." *Nature Communications* 14: 1–12.

Latos, B., T. Lefort, M. K. Flatau, et al. 2021. "Equatorial Waves Triggering Extreme Rainfall and Floods in Southwest Sulawesi, Indonesia." *Monthly Weather Review* 149: 1381–1401. https://journals.ametsoc.org/view/journals/mwre/149/5/MWR-D-20-0262.1.xml.

Lau, W. K.-M., and D. E. Waliser. 2012. *Intraseasonal Variability in the Atmosphere-Ocean Climate System*. Springer.

Lawton, Q. A., S. J. Majumdar, K. Dotterer, C. Thorncroft, and C. J. Schreck. 2022. "The Influence of Convectively Coupled Kelvin Waves on African Easterly Waves in a Wave-Following Framework." *Monthly Weather Review* 150: 2055–2072. https://journals.ametsoc.org/view/journals/mwre/150/8/MWR-D-21-0321.1.xml.

Li, T. 2014. "Recent Advance in Understanding the Dynamics of the Madden-Julian Oscillation." *Acta Meteorologica Sinica* 28: 1–33.

Liebmann, B., G. N. Kiladis, L. M. V. Carvalho, et al. 2009. "Origin of Convectively Coupled Kelvin Waves Over South America." *Journal of Climate* 22: 300–315. https://journals.ametsoc.org/view/journals/clim/22/2/2008jcli2340.1.xml.

Lin, H. 2022. "The Madden-Julian Oscillation." *Atmosphere-Ocean* 60: 338–359.

Liu, F., G. Huang, and M. Yan. 2015. "Role of SST Meridional Structure in Coupling the Kelvin and Rossby Waves of the Intraseasonal Oscillation." *Theoretical and Applied Climatology* 121: 623–629. https://doi.org/10.1007/s00704-014-1266-0.

Lu, W., and P.-C. Hsu. 2017. "Factors Controlling the Seasonality of the Madden-Julian Oscillation." *Dynamics of Atmospheres and Oceans* 78: 106–120.

Lubis, S. W., and M. R. Respati. 2021. "Impacts of Convectively Coupled Equatorial Waves on Rainfall Extremes in Java, Indonesia." *International Journal of Climatology* 41: 2418–2440. https://doi.org/10.1002/joc.6967.

Mahó, S. I., S. Vasylkevych, and N. Žagar. 2024. "Excitation of Mixed Ross By–Gravity Waves by Wave–Mean Flow Interactions on the Sphere." *Quarterly Journal of the Royal Meteorological Society* 150, no. 762: 2920–2936. https://doi.org/10.1002/qj.4742.

Maloney, E. D., Á. F. Adames, and H. X. Bui. 2019. "Madden–Julian Oscillation Changes Under Anthropogenic Warming." *Nature Climate Change* 9: 26–33.

Maloney, E. D., and D. L. Hartmann. 2000. "Modulation of Eastern North Pacific Hurricanes by the Madden–Julian Oscillation." *Journal of Climate* 13: 1451–1460. https://doi.org/10.1175/1520-0442(2000)013<1451:moenph>2.0.co;2.

Maloney, E. D., and J. T. Kiehl. 2002. "Mjo-Related Sst Variations Over the Tropical Eastern Pacific During Northern Hemisphere Summer." *Journal of Climate* 15: 675–689. https://doi.org/10.1175/1520-0442(2002)015<0675:mrsvot>2.0.co;2.

Matsuno, T. 1966. "Quasi-Geostrophic Motions in the Equatorial Area." *Journal of the Meteorological Society of Japan. Ser. II* 44: 25–43.

Mayta, V. C., G. N. Kiladis, J. Dias, P. L. S. Dias, and M. Gehne. 2021. "Convectively Coupled Kelvin Waves Over Tropical South America." *Journal of Climate* 34: 6531–6547. https://journals.ametsoc.org/view/journals/clim/34/16/JCLI-D-20-0662.1.xml.

Molinari, J., and D. Vollaro. 2000. "Planetary- and Synoptic-Scale Influences on Eastern Pacific Tropical Cyclogenesis." *Monthly Weather Review* 128: 3296–3307.

Mounier, F., G. N. Kiladis, and S. Janicot. 2007. "Analysis of the Dominant Mode of Convectively Coupled Kelvin Waves in the West African Monsoon." *Journal of Climate* 20: 1487–1503.

Nakamura, Y., and Y. N. Takayabu. 2022a. "Convective Couplings With Equatorial Rossby Waves and Equatorial Kelvin Waves. Part i: Coupled Wave Structures." *Journal of the Atmospheric Sciences* 79: 247–262.

Nakamura, Y., and Y. N. Takayabu. 2022b. "Convective Couplings With Equatorial Rossby Waves and Equatorial Kelvin Waves. Part II: Coupled Precipitation Characteristics." *Journal of the Atmospheric Sciences* 79: 2919–2933.

North, G. R., T. L. Bell, R. F. Cahalan, and F. J. Moeng. 1982. "Sampling Errors in the Estimation of Empirical Orthogonal Functions." *Monthly Weather Review* 110: 699–706. https://doi.org/10.1175/1520-0493(1982)110.

Pasch, R. J., and L. A. Avila. 1994. "Atlantic Tropical Systems of 1992." *Monthly Weather Review* 122: 539–548.

Peatman, S. C., A. J. Matthews, and D. P. Stevens. 2014. "Propagation of the Madden–Julian Oscillation Through the Maritime Continent and Scale Interaction With the Diurnal Cycle of Precipitation." *Quarterly Journal of the Royal Meteorological Society* 140: 814–825.

Perdigón-Morales, J., R. Romero-Centeno, B. S. Barrett, and P. Ordoñez. 2019. "Intraseasonal Variability of Summer Precipitation in Mexico: MJO Influence on the Midsummer Drought." *Journal of Climate* 32: 2313–2327. https://doi.org/10.1175/JCLI-D-18-0425.1.

Peyrillé, P., R. Roehrig, and S. Sanogo. 2023. "Tropical Waves Are Key Drivers of Extreme Precipitation Events in the Central Sahel." *Geophysical Research Letters* 50: e2023GL103715.

Rakhman, S., S. W. Lubis, and S. Setiawan. 2017. "Impact of Enso on Seasonal Variations of Kelvin Waves and Mixed Rossby-Gravity Waves." *IOP Conference Series: Earth and Environmental Science* 54: 012035.

Recalde-Coronel, G. C., B. Zaitchik, and W. K. Pan. 2020. "Madden–Julian Oscillation Influence on Sub-Seasonal Rainfall Variability on the West of South America." *Climate Dynamics* 54: 2167–2185. https://www.scopus.com/inward/record.uri?eid=2-s2.0-8507832556910.1007.

Roundy, P. E., and W. M. Frank. 2004. "A Climatology of Waves in the Equatorial Region." *Journal of the Atmospheric Sciences* 61: 2105–2132. https://doi.org/10.1175/1520-0469(2004)061<2105:ACOWIT>2.0.CO;2.

Russell, J. O., A. Aiyyer, J. D. White, and W. Hannah. 2017. "Revisiting the Connection Between African Easterly Waves and Atlantic Tropical Cyclogenesis." *Geophysical Research Letters* 44: 587–595.

Sakaeda, N., G. Kiladis, and J. Dias. 2020. "The Diurnal Cycle of Rainfall and the Convectively Coupled Equatorial Waves Over the Maritime Continent." *Journal of Climate* 33: 3307–3331.

Salas, H. D., J. Valencia, A. Builes-Jaramillo, and A. Jaramillo. 2022. "Synoptic Time Scale Variability in Precipitation and Streamflows for River Basins Over Northern South America." *Hydrology* 9: 59.

Seiki, A., S. Yokoi, and M. Katsumata. 2021. "The Impact of Diurnal Precipitation Over Sumatra Island, Indonesia, on Synoptic Disturbances and Its Relation to the Madden-Julian Oscillation." *Journal of the Meteorological Society of Japan. Ser. II* 99: 113–137.

Sena, A. C. T., Y. Peings, and G. Magnusdottir. 2022. "Effect of the Quasi-Biennial Oscillation on the Madden Julian Oscillation Teleconnections in the Southern Hemisphere." *Geophysical Research Letters* 49: e2021GL096105. https://www.scopus.com/inward/record.uri?eid=2-s2.0-85127457046.

Senior, N. V., A. J. Matthews, B. G. M. Webber, et al. 2023. "Extreme Precipitation at Padang, Sumatra Triggered by Convectively Coupled Kelvin Waves." *Quarterly Journal of the Royal Meteorological Society* 149: 2281–2300. https://doi.org/10.1002/qj.4506.

Serra, Y. L., G. N. Kiladis, and K. I. Hodges. 2010. "Tracking and Mean Structure of Easterly Waves Over the Intra-Americas Sea." *Journal of Climate* 23: 4823–4840.

Serra, Y. L., X. Jiang, B. Tian, J. Amador-Astua, E. D. Maloney, and G. N. Kiladis. 2014. "Tropical Intraseasonal Modes of the Atmosphere." *Annual Review of Environment and Resources* 39: 189–215.

Shreya, K., and E. Suhas. 2024. "A Survey of Westward-Propagating Mixed Rossby–Gravity Waves and Quantification of Their Association With Extratropical Disturbances." *Quarterly Journal of the Royal Meteorological Society* 150: 1752–1770.

Smith, G. L., and D. Rutan. 1994. "Spatial Variability of Outgoing Longwave Radiation." *Journal of Atmospheric Sciences* 51: 1808–1822. https://journals.ametsoc.org/view/journals/atsc/51/13/1520-0469_1994_051_1808_svoolr_2_0_co_2.xml.

Straub, K. H., and G. N. Kiladis. 2002. "Observations of a Convectively Coupled Kelvin Wave in the Eastern Pacific Itcz." *Journal of the Atmospheric Sciences* 59: 30–53. https://journals.ametsoc.org/view/journals/atsc/59/1/1520-0469_2002_059_0030_ooacck_2.0.co_2.xml.

Straus, D. M., D. I. V. Domeisen, S.-J. Lock, F. Molteni, and P. Yadav. 2023. "Intrinsic Predictability Limits Arising From Indian Ocean Madden–Julian Oscillation (MJO) Heating: Effects on Tropical and Extratropical Teleconnections." *Weather and Climate Dynamics* 4: 1001–1018. https://wcd.copernicus.org/articles/4/1001/2023/.

Suhas, E., J. M. Neena, and X. Jiang. 2020. "Exploring the Factors Influencing the Strength and Variability of Convectively Coupled Mixed Rossby-Gravity Waves." *Journal of Climate* 33: 9705–9719.

Takasuka, D., and M. Satoh. 2020. "Dynamical Roles of Mixed Rossby–Gravity Waves in Driving Convective Initiation and Propagation of the Madden–Julian Oscillation: General Views." *Journal of the Atmospheric Sciences* 77: 4211–4231.

Takasuka, D., T. Kohyama, H. Miura, and T. Suematsu. 2021. "MJO Initiation Triggered by Amplification of Upper-Tropospheric Dry Mixed Rossby-Gravity Waves." *Geophysical Research Letters* 48: 1–11.

Tarasova, L., R. Merz, A. Kiss, et al. 2019. "Causative Classification of River Flood Events." *WIREs Water* 6: e1353. https://doi.org/10.1002/wat2.1353.

Teruya, A. S. W., V. C. Mayta, B. Raphaldini, P. L. S. Dias, and C. R. Sapucci. 2024. "Tropical and Subtropical South American Intraseasonal Variability: A Normal-Mode Approach." *Meteorology* 3: 141–160.

Tiyas, D. A., S. W. Lubis, and S. Setiawan. 2022. "Kelvin Wave Activity in the Utls Over the Maritime Continent From Gps Ro Measurements." In *Proceedings of the International Conference on Radioscience, Equatorial Atmospheric Science and Environment and Humanosphere Science, 2021*, edited by E. Yulihastin, P. Abadi, P. Sitompul, and W. Harjupa, 83–96. Springer Nature Singapore.

Valencia, J., J. Yepes, J. F. Mejía, A. Builes-Jaramillo, and H. D. Salas. 2024. "Influence of Tropical Easterly Waves on the Chocojet During the 2019 Otrec Campaign." *Journal of Hydrometeorology* 25: 325–337.

van der Ent, R. J., and H. H. G. Savenije. 2011. "Length and Time Scales of Atmospheric Moisture Recycling." *Atmospheric Chemistry and Physics* 11: 1853–1863.

Webber, B. G. M., A. J. Matthews, and K. J. Heywood. 2010. "A Dynamical Ocean Feedback Mechanism for the Madden–Julian Oscillation." *Quarterly Journal of the Royal Meteorological Society* 136: 740–754. https://doi.org/10.1002/qj.604.

Wheeler, M., and G. N. Kiladis. 1999. "Convectively Coupled Equatorial Waves: Analysis of Clouds and Temperature in the Wavenumber–Frequency Domain." *Journal of the Atmospheric Sciences* 56: 374–399. https://journals.ametsoc.org/view/journals/atsc/56/3/1520-0469_1999_056_0374_ccewao_2.0.co_2.xml.

Wiggins, R. M., B. R. Lintner, Y. L. Serra, et al. 2023. "Tropical Easterly Waves Over Costa Rica and Their Relationship to the Diurnal Cycle of Rainfall." *Geophysical Research Letters* 50: e2023GL104159. https://doi.org/10.1029/2023GL104159.

Worku, L. Y., A. Mekonnen, and C. J. Schreck. 2020. "The Impact of Mjo, Kelvin, and Equatorial Rossby Waves on the Diurnal Cycle Over the Maritime Continent." *Atmosphere* 11, no. 7: 711. https://www.mdpi.com/2073-4433/11/7/711. https://doi.org/10.3390/atmos11070711.

Zemp, D. C., C. Schleussner, H. M. J. Barbosa, and A. Rammig. 2017. "Deforestation Effects on Amazon Forest Resilience." *Geophysical Research Letters* 44: 6182–6190.

Zemp, D. C., C.-F. Schleussner, H. M. J. Barbosa, et al. 2014. "On the Importance of Cascading Moisture Recycling in South America." *Atmospheric Chemistry and Physics Discussions* 14: 17479–17526.

Zhang, C. 2015. "Climate and Climate Change." In *Global Impacts of the Madden–Julian Oscillation*, 73–79. Elsevier.

Zhang, C., F. Adames, B. Khouider, B. Wang, and D. Yang. 2020. "Four Theories of the Madden-Julian Oscillation." *Reviews of Geophysics* 58, no. 3: e2019RG000685. https://doi.org/10.1029/2019RG000685.

Supporting Information

Additional supporting information can be found online in the Supporting Information section.

International Journal of Climatology

COUNTRY	SUBJECT AREA AND CATEGORY	PUBLISHER	SJR 2024
United Kingdom Universities and research institutions in United Kingdom Media Ranking in United Kingdom	Earth and Planetary Sciences └ Atmospheric Science	John Wiley and Sons Ltd	1.163 Q1 H-INDEX 201

PUBLICATION TYPE	ISSN	COVERAGE	INFORMATION
Journals	08998418, 10970088	1989-2025	Homepage How to publish in this journal jocproofs@wiley.com

SCOPE

The International Journal of Climatology aims to span the well established but rapidly growing field of climatology, through the publication of research papers, short communications, major reviews of progress and reviews of new books and reports in the area of climate science. The Journal's main role is to stimulate and report research in climatology, from the expansive fields of the atmospheric, biophysical, engineering and social sciences. Coverage includes: Climate system science; Local to global scale climate observations and modelling; Seasonal to interannual climate prediction; Climatic variability and climate change; Synoptic, dynamic and urban climatology, hydroclimatology, human bioclimatology, ecoclimatology, dendroclimatology, palaeoclimatology, marine climatology and atmosphere-ocean interactions; Application of climatological knowledge to environmental assessment and management and economic production; Climate and society interactions

Join the conversation about this journal

The International Journal of Climatology aims to span the well established but rapidly growing field of climatology, through the publication of research papers, short communications, major reviews of progress and reviews of new books and reports in the area of climate science. The Journal's main role is to stimulate and report research in climatology, from the expansive fields of the atmospheric, biophysical, engineering and social sciences. Coverage includes: Climate system science; Local to global scale climate observations and modelling; Seasonal to interannual climate prediction; Climatic variability and climate change; Synoptic, dynamic and urban climatology, hydroclimatology, human bioclimatology, ecoclimatology, dendroclimatology, palaeoclimatology, marine climatology and atmosphere-ocean interactions; Application of climatological knowledge to environmental assessment and management and economic production; Climate and society interactions

Join the conversation about this journal

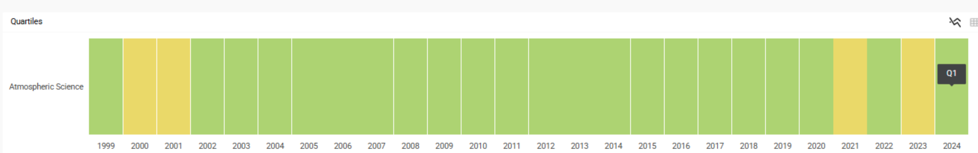

FIND SIMILAR JOURNALS

1	2	3	4	5
Weather and Climate Extremes	Atmospheric and Oceanic Science Letters	Climate Dynamics	Plateau Meteorology	Journal of Meteorological Research
NLD	GBR	DEU	CHN	CHN
85% similarity	81% similarity	79% similarity	78% similarity	76% similarity

SJR · Citations per document

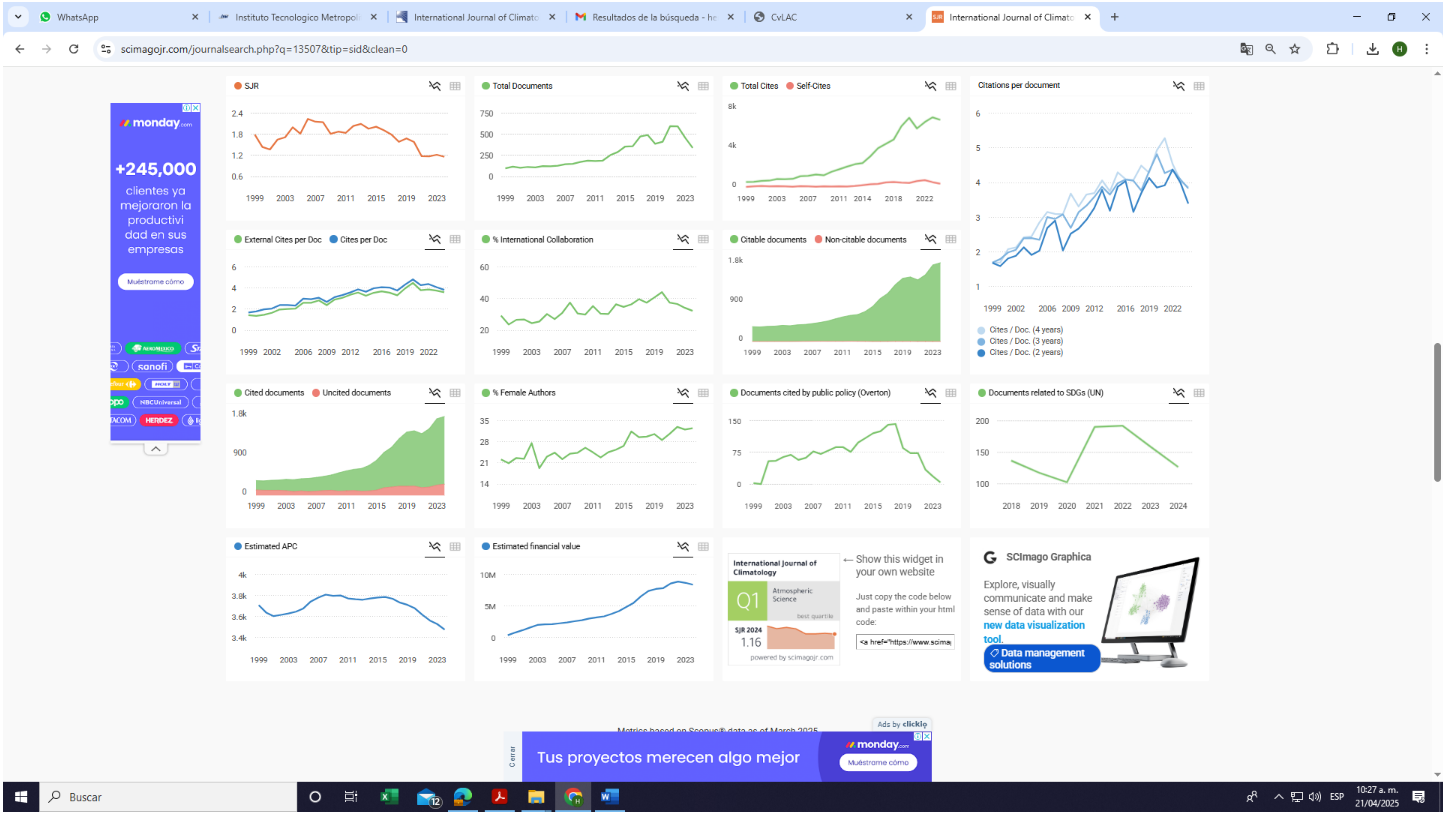
WhatsApp
Instituto Tecnologico Metropol
International Journal of Climat
Resultados de la búsqueda - h
CvLAC
International Journal of Climat
scimagojr.com/journalsearch.php?q=13507&tip=sid&clean=0
SJR
Total Documents
Total Cites
Self-Cites
Citations per document
External Cites per Doc
Cites per Doc
% International Collaboration
Citable documents
Non-citable documents
Cites / Doc. (4 years)
Cites / Doc. (3 years)
Cites / Doc. (2 years)
Cited documents
Uncited documents
% Female Authors
Documents cited by public policy (Overton)
Documents related to SDGs (UN)
Estimated APC
Estimated financial value
International Journal of Climatology
Q1
Atmospheric Science
best quartile
SJR 2024
1.16
powered by scimagojr.com
← Show this widget in your own website
Just copy the code below and paste within your html code:
<a href="https://www.scima
SCImago Graphica
Explore, visually communicate and make sense of data with our new data visualization tool.
Data management solutions
monday.com
+245,000
clientes ya mejoraron la productividad en sus empresas
Muéstrame cómo
sanofi
HERDEZ
Tus proyectos merecen algo mejor
Ads by clickio
Buscar
ESP
10:27 a. m.
21/04/2025